

# Strain partitioning and fabric evolution as a correlation tool : the example of the Eclogitic Micaschists Complex in the Sesia-Lanzo Zone (Monte Mucrone-Monte Mars, Western Alps, Italy)

Autor(en): **Zucali, Michele / Spalla, Maria Iole / Gosso, Guido**

Objektyp: **Article**

Zeitschrift: **Schweizerische mineralogische und petrographische Mitteilungen  
= Bulletin suisse de minéralogie et pétrographie**

Band (Jahr): **82 (2002)**

Heft 3

PDF erstellt am: **24.09.2024**

Persistenter Link: <https://doi.org/10.5169/seals-62374>

## **Nutzungsbedingungen**

Die ETH-Bibliothek ist Anbieterin der digitalisierten Zeitschriften. Sie besitzt keine Urheberrechte an den Inhalten der Zeitschriften. Die Rechte liegen in der Regel bei den Herausgebern.

Die auf der Plattform e-periodica veröffentlichten Dokumente stehen für nicht-kommerzielle Zwecke in Lehre und Forschung sowie für die private Nutzung frei zur Verfügung. Einzelne Dateien oder Ausdrucke aus diesem Angebot können zusammen mit diesen Nutzungsbedingungen und den korrekten Herkunftsbezeichnungen weitergegeben werden.

Das Veröffentlichen von Bildern in Print- und Online-Publikationen ist nur mit vorheriger Genehmigung der Rechteinhaber erlaubt. Die systematische Speicherung von Teilen des elektronischen Angebots auf anderen Servern bedarf ebenfalls des schriftlichen Einverständnisses der Rechteinhaber.

## **Haftungsausschluss**

Alle Angaben erfolgen ohne Gewähr für Vollständigkeit oder Richtigkeit. Es wird keine Haftung übernommen für Schäden durch die Verwendung von Informationen aus diesem Online-Angebot oder durch das Fehlen von Informationen. Dies gilt auch für Inhalte Dritter, die über dieses Angebot zugänglich sind.

# Strain partitioning and fabric evolution as a correlation tool: the example of the Eclogitic Micaschists Complex in the Sesia-Lanzo Zone (Monte Mucrone-Monte Mars, Western Alps, Italy)

by Michele Zucali<sup>1</sup>, Maria Iole Spalla<sup>1,2</sup> and Guido Gosso<sup>1,2</sup>

## Abstract

The structural history of the Eclogitic Micaschists Complex of the Sesia-Lanzo Zone (Austroalpine domain, Western Italian Alps), along the Monte Mucrone-Mombarone section, reveals seven superposed deformation phases detected by foliation mapping. Superposed meso- and microstructures have been used as correlation tool to interpret the progression of the tectono-metamorphic development. A pre-Alpine stage (pre-D<sub>1</sub>), marked by high temperature/low pressure mineralogical assemblages, is preserved within metapelites (S<sub>pre-1</sub>). Within the meta-intrusive body of Monte Mars-Monte Mucrone the pre-D<sub>1</sub> relics consist of undeformed lenses with igneous textures. S<sub>1</sub> Alpine foliation developed under HP/LT conditions; S<sub>2</sub> foliation is the most penetrative fabric and is marked by eclogite facies mineralogical assemblages; D<sub>3</sub> developed under eclogite facies conditions and is locally recorded. D<sub>4</sub> localised shear zones are marked by blueschist facies assemblages. D<sub>5</sub> folds, the most penetrative isoclinal fold system, developed during retrogradation under greenschist facies conditions. Thermo-barometric estimates indicate that rocks re-equilibrated at P = 0.3 ± 0.05 GPa and T = 720 ± 48 °C, during pre-D<sub>1</sub> deformation, whereas the early deformational history (D<sub>2</sub> and D<sub>3</sub>) occurred at P ≥ 1.3 GPa and T = 500–600 °C. During exhumation these rocks re-equilibrated at P ≤ 1.5 GPa and T ≤ 600 °C during D<sub>4</sub> and at P ≤ 0.8 GPa and T ≤ 350 °C during D<sub>5</sub>. The resulting P-T-d-t path indicates that the T/depth ratios during the eclogitic peak (~10 °C km<sup>-1</sup>) and the exhumation path (≤14 °C km<sup>-1</sup>) are very low. Geochronological data suggest that exhumation took place at rates ≥1.4 mm year<sup>-1</sup>. The present day structural and metamorphic setting highlights the relationships between fabric evolution and the progression of the metamorphic transformations. These relations show that during the Alpine evolution, within an area of ~30 km<sup>2</sup>, only small rock domains escaped the structural (~6%) and the metamorphic (~0.3%) re-equilibrations; on the other hand, in this subducted slice of continental crust, the S<sub>2</sub> dominant fabric (~70% of the rock volume) developed under eclogitic conditions, whereas during retrograde evolution, textural (~6.3%) and metamorphic (~3%) re-equilibrations, associated with large scale folding, were restricted to smaller areas.

*Keywords:* fabric evolution, tectono-metamorphic correlation, subduction metamorphism, exhumation metamorphism, Western Alps.

## 1. Introduction

The most effective method for a correlation of deformation and metamorphic events in polydeformed and polymetamorphic terrains is the use of several tools such as microstructural analysis, stable mineral assemblages marking superposed fabrics and absolute age data (TURNER and WEISS, 1963; PARK, 1969; HOBBS et al., 1976; VAN ROERMUND et al., 1979; WILLIAMS, 1985; PASSCHIER et al., 1990; JOHNSON and VERNON, 1995; SPALLA et al., 2000). Examples from different metamorphic

belts have shown that the heterogeneity of deformation (JOHNSON, 1990; JOHNSON and DUNCAN, 1992; JOHNSON and VERNON, 1995) bears a systematic relationship with the dominant metamorphic imprint (SPALLA and GOSSO, 1999; SPALLA et al., 2000). Classically, metamorphic complexes have been distinguished on the basis of their lithological homogeneity and metamorphic overprint, while P-T-d-t reconstructions demonstrate different metamorphic overprints within the same basement unit (e.g. POGNANTE, 1991; SPALLA et al., 1996 in the Western Alps).

<sup>1</sup> Dipartimento di Scienze della Terra, Università di Milano, Via Mangiagalli 34, I-20133 Milano, Italy. <Michele.Zucali@unimi.it>, <Iole.Spalla@unimi.it>, <Guido.Gosso@unimi.it>

<sup>2</sup> CNR-Centro di Studio per la Geodinamica Alpina e Quaternaria, Via Mangiagalli 34, I-20133 Milano, Italy.

During every single deformation event, mineral transformation and strain heterogeneity may generate new different fabrics (e.g. coronitic, tectonic and mylonitic fabrics); where they are marked by new mineralogical assemblages, the latter indicates specific P-T conditions, which may occur along strain gradients and represent examples of progressive heterogeneous strain. Coronitic fabrics are interpreted as places where isolated structural and metamorphic relics are preserved and where a sequence of metamorphic transformations may be established. Tectonic fabrics represent a moderate deformational overprint and allow inferring the chronological succession of deformational events from coronitic to fully re-equilibrated mylonitic domains in which usually none of the older relics are present. In addition, the model of deformation partitioning at the grain size scale (e.g. BELL et al., 1986) allows relating granular scale deformation stages to successive kinematic stages, from crenulation to complete obliteration of original fabric (BELL and RUBENACH, 1983; BELL and HAYWARD, 1991). Such kinematic stages can be correlated to the growth of reaction products of metamorphic transformations, distinguishing between fabrics dominantly supported by old minerals, slightly re-arranged by new minerals (coronitic microstructure of the fabric) and fabrics entirely marked by the new metamorphic assemblage (S or S/L-tectonite and mylonite). The field correlation of progressive strain states (coronitic, tectonic and mylonitic fabrics) and the related reacting volumes represents the basis of correlation of the tectono-metamorphic history (e.g. GAZZOLA et al., 2000). The structural and metamorphic correlation at the regional scale may separate the volumes, which have experienced a homogeneous tectono-thermal evolution. In this contribution, it is shown how a structural-petrographic map may support tectono-metamorphic correlation in the polymetamorphic terrain of the inner Sesia-Lanzo Zone (SLZ). Detailed (1:5'000, ZUCALI in press) lithologic and structural mapping demonstrates how present day lithological associations result from complex interaction between characteristics of the original protoliths, their tectono-metamorphic evolution, strain partitioning, and progressive mechanical and mineralogical re-equilibration. This new structural-petrographic map consists of a network of foliation traces developed under different metamorphic conditions and shows: (i) progressive rotation of structures; (ii) incompatibility of parageneses associated with different fabrics; (iii) finite strain gradients produced by strain partitioning during each stage of the polyphased tectono-metamorphic evolution.

Mineral abbreviations used are from KRETZ (1973, 1983, 1994) except for white mica (Wm).

## 2. Geological setting

The SLZ belongs to the Austroalpine domain of the Western Italian Alps and consists of two main elements distinguished on the basis of their lithological affinity (e.g. COMPAGNONI et al., 1977): an upper element, comprising metapelites and metabasites with a dominant metamorphic imprint under amphibolite/granulite facies conditions of pre-Alpine age, "the II Zona Diorito-Kinzigitica" (IIDK), and a lower element, consisting of metapelites, metagranitoids and metabasites, divided into two metamorphic complexes: the Gneiss Minuti Complex (GMC), showing a dominant Alpine metamorphic imprint under greenschist facies conditions, and the Eclogitic Micaschists Complex (EMC) showing a dominant Alpine imprint under eclogite facies conditions. VENTURINI et al. (1991, 1994) proposed a different subdivision of the SLZ into three elements: a polymetamorphic basement complex (GMC and EMC), a monometamorphic basement complex (Bonze and Scalaro Units) and a pre-Alpine high temperature basement complex (IIDK). They based the separation of a monometamorphic complex on the close association of MORB-type metabasites, marbles and quartzites, suggesting a possible Mesozoic age for the protoliths. Successive radiometric determinations (RUBATTO, 1998; RUBATTO et al., 1999) yielded absolute igneous ages of  $350 \pm 10$  Ma (U-Pb method on zircons) for these MORB-type metabasites. These new results make the monometamorphic nature of such a unit questionable. A new petrographic-structural map was produced in a sector of the most internal part of the EMC, located at the divide between Valle dell'Elvo and Val di Gressoney to the north and between lower Val d'Aosta and Valle dell'Elvo to the south (Fig. 1). Some authors suggest abandoning of the classical SLZ subdivision into metamorphic complexes, recognising that their main differences consist of fabric gradients and different rates of metamorphic transformations (SPALLA et al., 1991; STÜNITZ, 1989).

Lithologies are physically continuous from the Monte Mucrone to Colma di Mombarone and Ivozio. They consist of small lenses of biotite-garnet-Al silicates-metapelites ("kinzigitites"), dominant garnet-omphacite-NaCa amphibole-metapelites, omphacite-glaucophane-meta-quartzdiorite bodies, metagranitic intercalations, lenses of metabasites (amphibole-bearing eclogites and eclogites), pure and impure marbles, kyanite-chlori-

toid-garnet-quartzites, metre-size peridotitic lenses and andesitic dykes (DAL PIAZ et al., 1972; COMPAGNONI and MAFFEO, 1973; POGNANTE et al., 1980; HY, 1984; KOONS et al., 1987; VENTURINI, 1995); metagranitoids and meta-quartzdiorite of the Monte Mars constitute the western part of the Monte Mucrone metaintrusive body (Fig. 2); from

this latter an age of 293  $\pm$  1–2 Ma has been derived using U–Pb method on zircons (BUSSY et al., 1998). All lithologies, apart from the Oligocene andesitic dykes (DAL PIAZ et al., 1979; DE CAPITANI et al., 1979; BECCALUVA et al., 1983), show a penetrative Alpine metamorphic imprint, whereas pre-Alpine assemblages are scanty. The age of

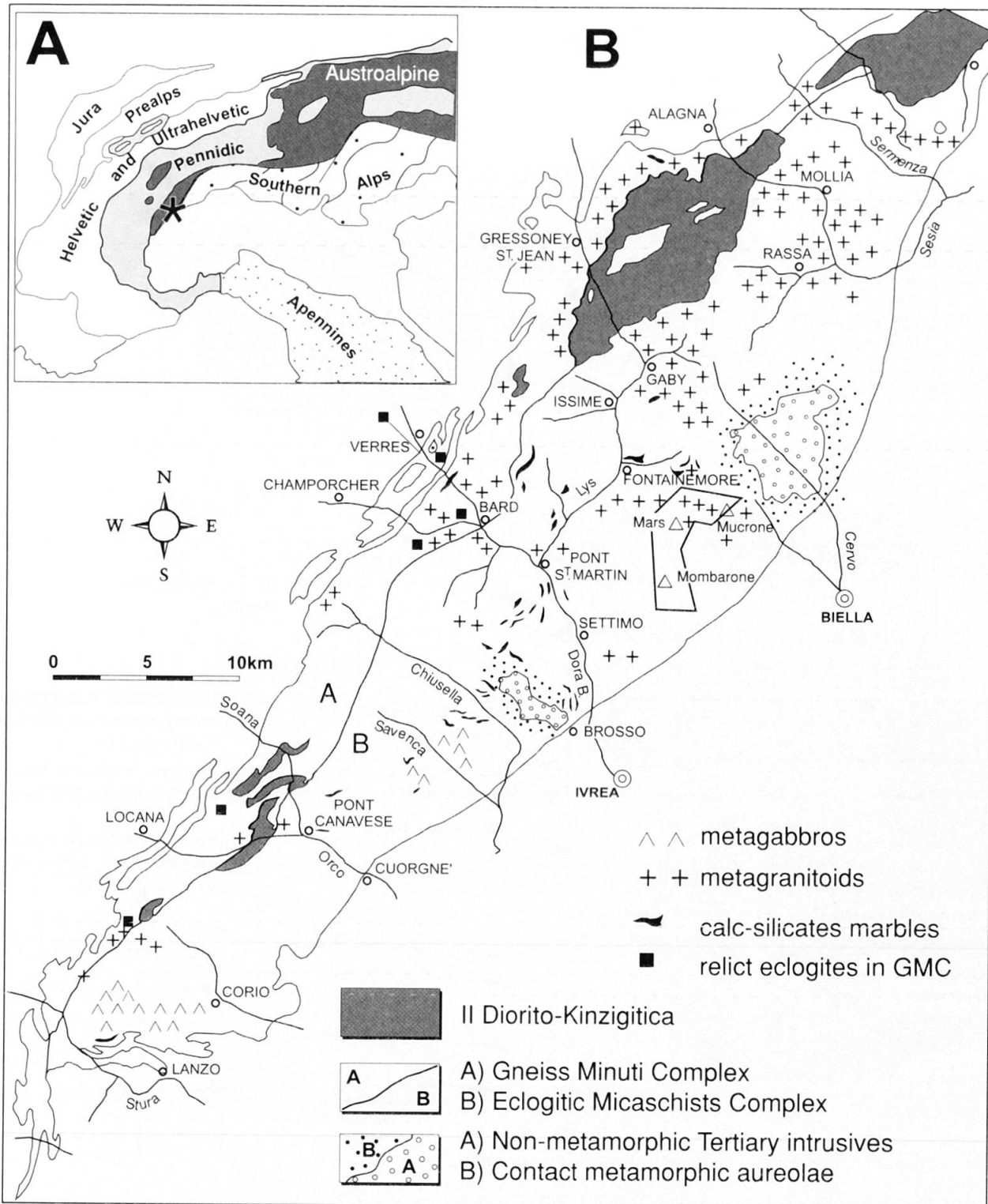


Fig. 1 (A) Tectonic outline of the Alpine chain. Asterisk locates the Sesia-Lanzo Zone. (B) Simplified geological map of the Sesia-Lanzo Zone.



the Alpine eclogitic metamorphic evolution of the SLZ has been dated as Late Cretaceous–Early Paleocene: INGER et al. (1996) dated the eclogitic re-equilibration of the Monte Mucrone metaquartzdiorite ( $63.0 \pm 1.3$  Ma, using Rb–Sr method on white mica), the surrounding eclogites ( $68.6 \pm 3.1$  Ma, using Rb–Sr method on white mica) and metapelites ( $53.8 \pm 1.8$  Ma, using Rb–Sr method on white mica) and the Monte Mars

metapelites ( $68.8 \pm 2.2$  Ma, using Rb–Sr method on white mica). RUFFET et al. (1997), showed an age convergence of 64–66 Ma for the high pressure (HP) metamorphic event (Rb–Sr and  $^{40}\text{Ar}$ – $^{39}\text{Ar}$  on phengite); DUCHENE et al. (1997) obtained an age of  $69.2 \pm 2.7$  Ma for the eclogites of Lillianes-Fontainemore, using Lu–Hf method on garnet and pyroxene. RUBATTO (1999) dated the Alpine eclogite facies zircons of the Monte

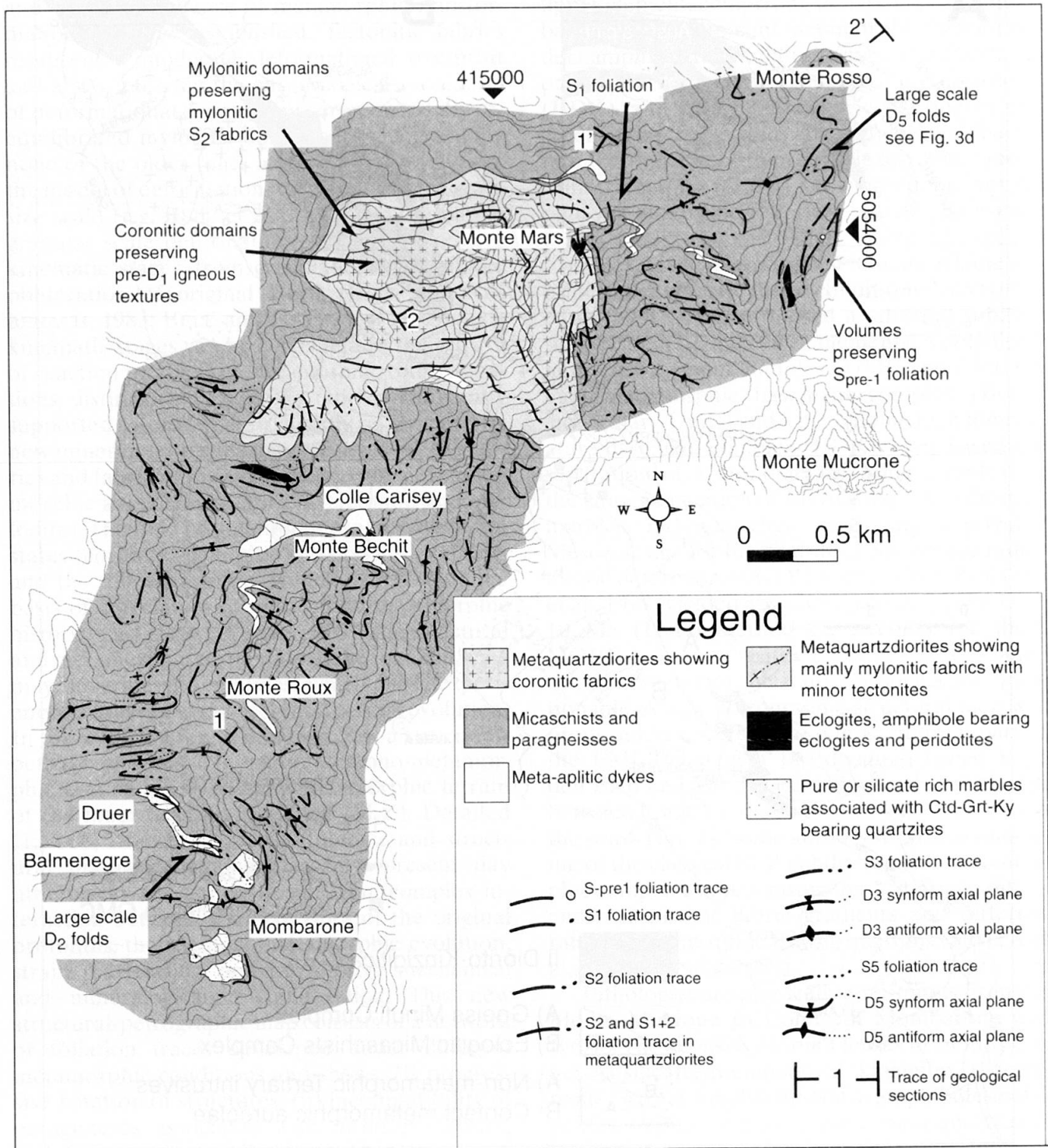


Fig. 2 Petrographic-structural map of the Monte Rosso-Monbarone divide, between Biella, Val di Gressoney and lower Val d'Aosta.

Mucrone meta-quartzdiorite at  $65 \pm 5$  Ma (U-Pb method).

Many authors defined the relationships between deformation and metamorphism from the external to the internal part of the Central and Southern Sesia-Lanzo Zone (GOSSO, 1977; GOSSO et al., 1979; POGNANTE et al., 1980; PASSCHIER et al., 1981; SPALLA et al., 1983; WILLIAMS and COMPAGNONI, 1983; HY, 1984; VUICHARD, 1986; RIDLEY, 1989; STÜNITZ, 1989; ILDEFONSE et al., 1990; LARDEAUX and SPALLA, 1991; VENTURINI et al., 1991; INGER and RAMSBOTHAM, 1997). The resulting outline for the EMC consists of a pre-Alpine structural and metamorphic re-equilibration, developed from granulite to amphibolite facies conditions, followed by an Alpine overprint under eclogite to blueschist facies conditions and by a greenschist facies retrogradation (Table 1). From Table 1 it can be noted that the chronological sequence of superposed structures and the correspondence between deformation phases and compatible metamorphic assemblages is not univocal, even considering adjacent areas of a single metamorphic complex (e.g. the EMC). Actually, a blueschist foliation can occur as a prograde foliation predating the eclogitic fabric or as a post-eclogitic foliation in adjacent portions of the EMC (POGNANTE et al., 1980; WILLIAMS and COMPAGNONI, 1983; VENTURINI et al., 1991). In places, the eclogitic structures consist of composite foliations or superposed folds and foliations and are the earliest fabrics (HY, 1984; ILDEFONSE et al., 1990; VENTURINI et al. 1991; INGER and RAMSBOTHAM, 1997); eclogitic fabrics are in place overprinted by a retrograde blueschist imprint. In other cases, the eclogitic fabric coincides with the earlier penetrative foliation ( $S_1$ ) (GOSSO, 1977; GOSSO et al., 1979; POGNANTE et al., 1980; PASSCHIER et al., 1981). The retrograde blueschist and greenschist evolution occurred during polyphase deformation. The 1:5'000 map in Fig. 2 has been produced where the meso-scale correlation between mineral assemblages and foliations is facilitated by coarse grain size. Overprinting relationships between structures and metamorphic imprints in different chemical systems have been used to constrain P-T conditions and establish a correlation within the mapped area.

### 3. Meso-structures and their mineralogical support

The mapping of foliations, lineations, fold systems and shear zones reveals an array of lozenge-shaped bodies that have progressively formed during the entire tectonic history and represent a mosaic of heterogeneous finite strain domains

(Figs. 2 and 11). The map (Fig. 2) shows that some lozenges of the meta-quartzdiorites have largely escaped deformation (coronitic fabric = low strain); such lozenge-shaped bodies are wrapped by a network of superposed foliations ( $S$  or  $S/L$  tectonic fabric = intermediate strain) and shear zones (mylonitic fabrics = high strain) that developed during each phase of deformation. Mineral assemblages marking the fabric elements may consequently be related to the relative timing or kinematic sequence of mesostructures within each lithology (phases of deformation e.g.  $D_{pre-1}$ ,  $D_1$ ,  $D_2$ ). It is thus possible to show the finite strain gradients in maps for each phase of deformation, to discriminate and quantify the metamorphic conditions under which they developed. This study presents important insights on the structural level and geodynamic environment of deformational events.

In Figure 2 and Table 2 successive and superposed mesostructures and their relationships are schematically summarized; in Table 2 the mineral assemblages supporting superposed fabrics are specified. In Figures 3–4 the representative mesostructures are located in the regional scale structural framework. The orientation of fabric elements is plotted in Schmidt diagrams (Fig. 5).

$D_{pre-1}$  structures are characterised by a  $S_{pre-1}$  foliation within metapelites (Table 2) and by relic igneous textures in meta-quartzdiorites (Fig. 3a and Table 2).  $D_{pre-1}$  structures are preserved within lozenges of 1 to 100 m in size (Fig. 2).

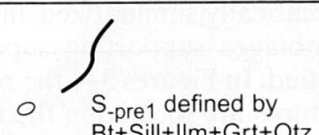
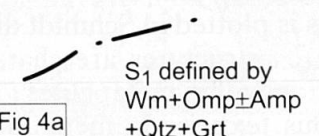
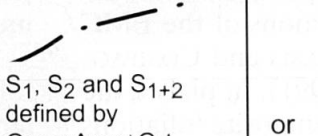
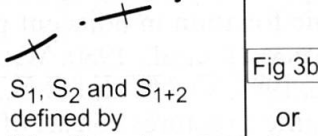
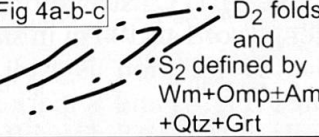
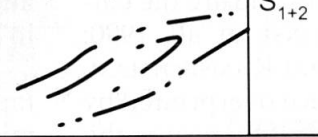
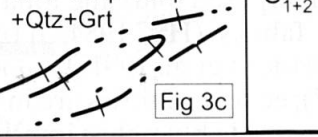
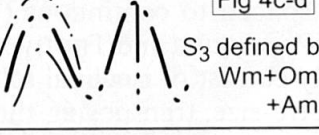
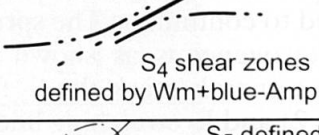
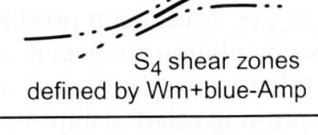
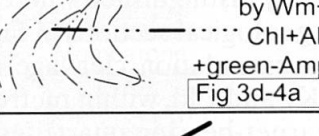
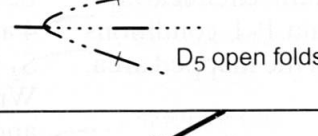
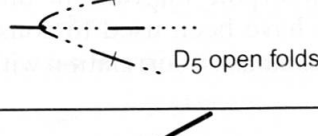
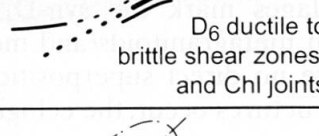
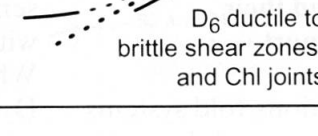
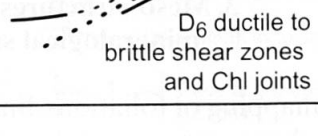
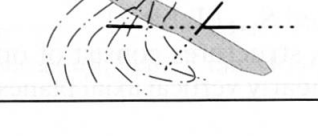
The  $S_1$  foliation is well preserved in metapelites (Fig. 4) and is marked by eclogite facies minerals (Table 2).  $S_1$  is a differentiated foliation, from spaced to continuous (TWISS and MOORE, 1993; PASSCHIER and TROUW, 1996).  $D_2$  structures mainly consist of isoclinal folds, from centimetre to metre-size, transposing the  $S_1$  foliation into a new penetrative  $S_2$  axial plane foliation, that is spaced to continuous. The spread of  $D_2$  structures is heterogeneous as shown in Fig. 2. Eclogite facies minerals mark the  $S_2$  foliation (Fig. 4 and Table 2) and  $L_2$  stretching lineation.  $S_1$  and  $S_2$  can be clearly distinguished where  $D_2$  folds occur (Fig. 4 and geological sections in Figs. 3–4 and Table 2).  $S_2$  is a crenulation cleavage marked by SPO of Wm, Ky and Cld, within metre-size lenses of mica and garnet-bearing quartzites. Eclogite facies assemblages mark the syn- $D_1$  and  $D_2$  foliations within metagranitoids and metabasics (Table 2). Where no direct superposition between  $D_1$  and  $D_2$  structures occur, the eclogitic foliations within metabasites and meta-quartzdiorites have been labelled  $S_{1+2}$  (Table 2).

$D_3$  structures consist of open to isoclinal folds with nearly vertical axial planes (Fig. 4 and Table 2).

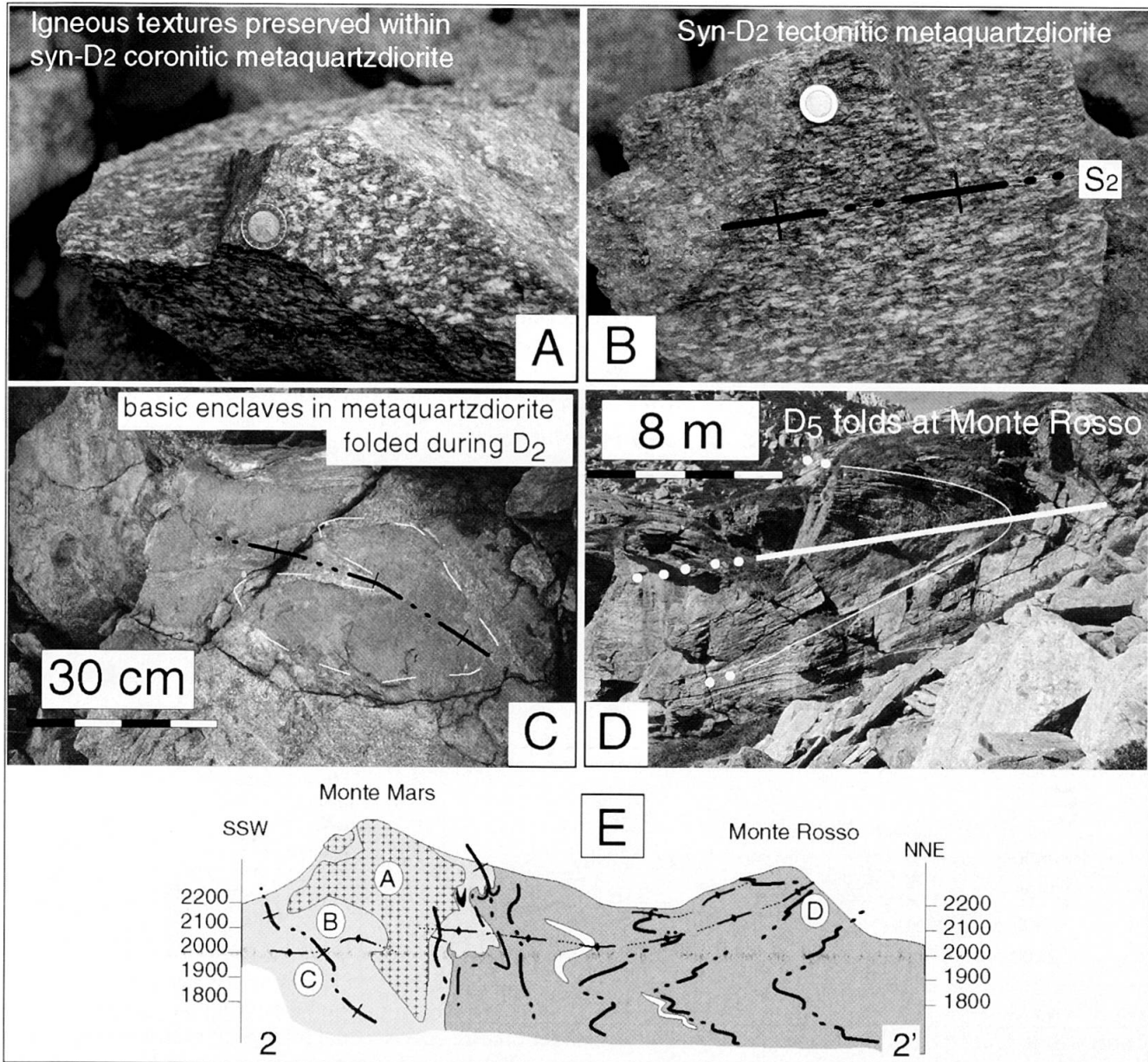
Table 1 Relationships between deformation and metamorphism in the EMC of the Sesia-Lanzo Zone, according to published and present work: (1) GOSSO, 1977; (2) POGNANTE et al., 1980; (3) PASSCHIER et al., 1981; (4) WILLIAMS and COMPAGNONI, 1983; (5) HY, 1984; (6) RIDLEY, 1989; (7) ILDEFONSE et al., 1990; (8) VENTURINI et al., 1991; (9) INGER and RAMSBOTHAM, 1997.

Eclogitic Micaschists Complex					
References	Pre-Alpine	Blueschist	Eclogite	Blueschist	Greenschist
(1)			D1	D2	D3
(2)		D0	D1	D2	D3
(3)	D0		D1	D2	D3+D4
(4)	D1	D2	D3	D4	D5
(5)	D0		D1 + D2 ----- > D2		
(6)			D1	D2	D3
(7)			D1 + D2 ----- > D2		D3
(8)	D0	D1	D2+D3		D4
(9)	D0		D1+D2	D3	static
This work	pre-D1		D1 + D2 + D3	D4	D5+D6

Table 2 Schematic representation of mesostructures developed in metapelites, metabasites and meta-intrusives during pre-Alpine and Alpine evolution.

Deformation phases	Metapelites	Metabasites	Metaintrusives
<b>pre-D1</b>	 S <sub>pre1</sub> defined by Bt+Sill+Ilm+Grt+Qtz	no pre-D1 structures	igneous texture Fig 3a
<b>D1</b>	 S <sub>1</sub> defined by Wm+Omp±Amp+Qtz+Grt Fig 4a	 S <sub>1</sub> , S <sub>2</sub> and S <sub>1+2</sub> defined by Omp+Amp±Grt	 S <sub>1</sub> , S <sub>2</sub> and S <sub>1+2</sub> defined by Wm+Omp+Amp+Qtz+Grt Fig 3b or S <sub>1+2</sub>
<b>D2</b>	 D <sub>2</sub> folds and S <sub>2</sub> defined by Wm+Omp±Amp+Qtz+Grt Fig 4a-b-c		 Fig 3c or S <sub>1+2</sub>
<b>D3</b>	 S <sub>3</sub> defined by Wm+Omp+Amp Fig 4c-d	no D3 structures	no D3 structures
<b>D4</b>	 S <sub>4</sub> shear zones defined by Wm+blue-Amp	no D4 structures	 S <sub>4</sub> shear zones defined by Wm+blue-Amp
<b>D5</b>	 S <sub>5</sub> defined by Wm+Chl+Ab+green-Amp Fig 3d-4a	 D <sub>5</sub> open folds	 D <sub>5</sub> open folds
<b>D6</b>	 D <sub>6</sub> ductile to brittle shear zones and Chl joints	 D <sub>6</sub> ductile to brittle shear zones and Chl joints	 D <sub>6</sub> ductile to brittle shear zones and Chl joints
<b>andesitic dykes</b>		no dykes cut metabasites	no dykes cut metaintrusives





**Fig. 3** (A) Slightly deformed meta-quartzdiorites at Lago Goudin. Qtz grains, still preserving igneous texture, are surrounded by Omp, Zo and Wm replacing Pl and Bt igneous sites. (B)  $S_2$  foliation within meta-quartzdiorites defined by SPO of Wm + Ep  $\pm$  Omp and Amp. (C) Basic enclave folded during  $D_2$  within meta-quartzdiorites at Lago Goudin (Monte Mars).  $S_2$  foliation within meta-quartzdiorites marks the axial plane. (D) Large scale  $D_5$  fold at Monte Rosso within Omp and Gln-bearing micaschists. (E) Geological cross section between Monte Mars and Monte Rosso (2–2' in Fig. 2). Circled letters locate the photographs. Symbols as in Fig. 2.

Locally a new centimetre-size differentiated axial plane foliation ( $S_3$ ) develops.

$D_4$  structures consist of thin shear zones (up to 10 centimetre in width), both within the meta-intrusives of the Monte Mars-Monte Mucrone and in the metapelites, and occur on pre- $D_4$  coronitic and tectonic fabrics.

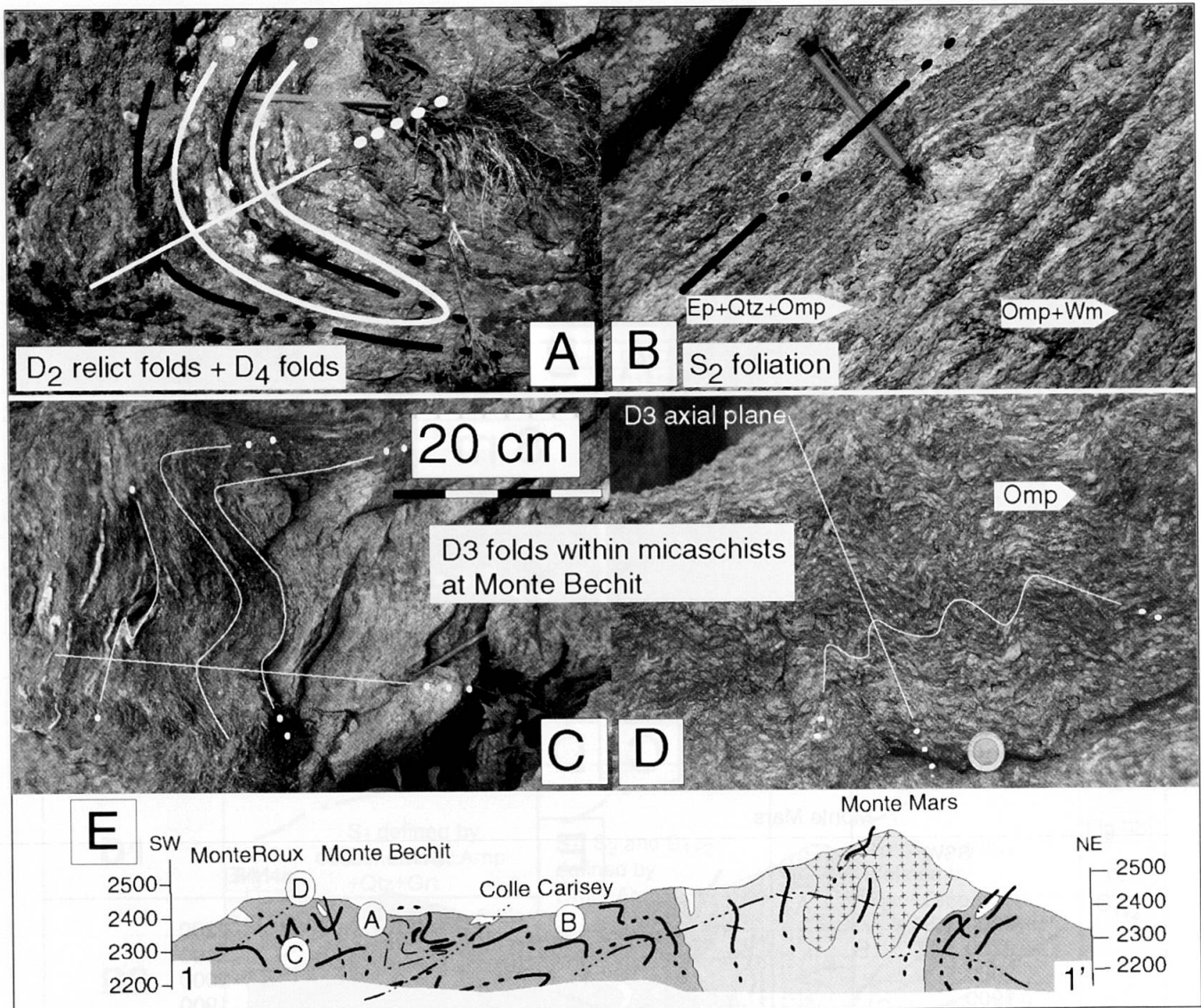
$D_5$  structures represent the most recurrent geometric situation at different scales (Figs. 3d–4a and Table 2); they are open to isoclinal folds, ranging in size from centimetre to kilometre, with a

sub-horizontal dip of the axial plane (Fig. 3d), locally associated with a differentiated axial plane foliation ( $S_5$ ).

$D_6$  is characterised by local centimetre-size ductile to brittle shear zones not accompanied by new mineral transformations. Large-scale  $D_6$  deformation also results in a gentle and large-scale undulation (Table 2).

Oligocenic andesitic dykes crosscut all these structures fixing the minimal age of the deformation history.





**Fig. 4** (A) Superposition (type 3 of RAMSAY, 1967) of  $D_5$  onto  $D_2$  folds in Omp-Gln-bearing micaschists at Colle Carisey.  $S_1$  is defined by SPO of Omp and Wm.  $D_2$  fold is a centimetre-size isoclinal fold (right bottom) wrapped by the  $S_2$  foliation.  $S_2$  foliation is still marked by Omp and Wm SPO.  $D_5$  fold is a metre-size open fold with a gentle dipping axial plane and without axial plane foliation. (B)  $S_2$  foliation within metapelites marked by SPO of Wm, Omp and Amp (dark grey); centimetre thick layers contain Ep and Qtz  $\pm$  Grt (light grey). (C)  $S_2$  foliation in the quartz-rich micaschists associated with rootless  $D_2$  fold hinges, bent by  $D_3$  folding at Colle Carisey-Monte Bechit (photograph rotated by  $90^\circ$ ). (D)  $S_2$  foliation in the quartz-rich micaschists at Monte Bechit, marked by SPO of Wm, Qtz and large Omp porphyroblasts, crenulated during  $D_3$ . (E) Geological cross section between Monte Mars and Monte Rosso (1-1' in Fig. 2). Circled letters locate the photographs. Symbols as in Fig. 2.

#### 4. Microstructural Analysis

Our microstructural analysis aims at defining the relationships between deformation and metamorphism. We use the heterogeneous nature of deformation (BELL, 1981; BELL and RUBENACH, 1983) to recognise favourable sites for pre-, syn- and post-kinematic growth during each phase of deformation. In Figures 6-8 the relationships between microstructural evolution and metamorphic growth are summarized. Here the distinction of successive stages of development of the  $S_2$  ec-

logitic foliation, from crenulation to complete decrenulation has been used to establish links between rate of deformation and metamorphic transformation. The record of the different stages of  $S_2$  development is complete in metapelites, but incomplete in meta-quartzdiorites, metabasites, and quartzites. Stages 1, 2 and 3 describe, within metapelites, three steps from  $S_1$  crenulation (stage 1) to  $S_2$  continuous foliation (stage 3), where no structural relics (e.g. microfold hinges) are preserved.

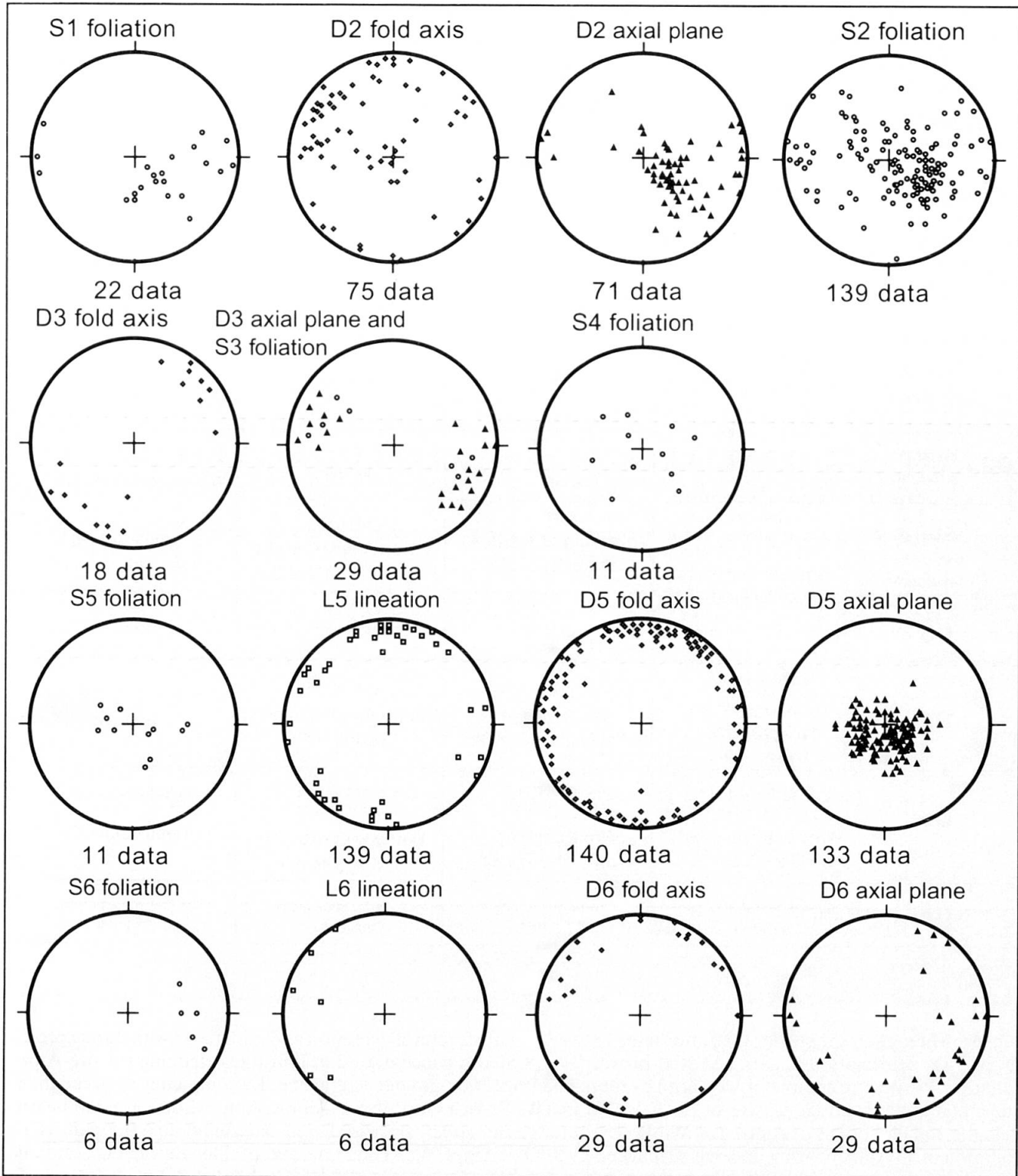


Fig. 5 Schmidt projections (lower hemisphere) of fabric elements orientations within metapelites, meta-quartzdiorites, metabasites and quartzites.

#### 4.1. PRE-ALPINE EVOLUTION

**Pre-D<sub>1</sub>** Within a small lens of kinzigitic metapelite, north of Lago Mucrone (Fig. 2), granulitic pre-Alpine minerals define a discontinuous layering (Fig. 6a); their modal amount is  $\leq 15\%$ .

Red-brown Bt, Sil, Ilm and rare WmI constitute the

films, whereas the lithons contain GrtI porphyroblasts, Kfs, ex-Pl (replaced by Cpx and WmII aggregates), Qtz and decussate arcs of red-brown Bt; Bt, Ilm, Qtz and Pl inclusions occur in GrtI.

The inferred pre-D<sub>1</sub> mineral association in metapelites is:

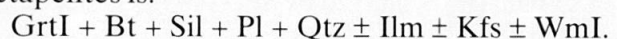


Table 3 Minerals and mineralogical assemblages characterizing each fabric during the pre-Alpine and Alpine evolution in metapelites, metabasites, meta-intrusives and quartzites.

Deformation phases	Metapelites	Metabasites	Metaintrusives	Cld-Ky-Grt quartzites
<b>pre-D1</b>	GrtI+Bt+Sil+Pl+Qtz ±Ilm±Kfs±WmI in tectonic fabrics ( $S_{pre1}$ )	Ti-rich Amp no preserved pre-D <sub>1</sub> fabrics	Ti-rich Amp igneous textures	no relics
<b>D1</b>	in coronitic fabrics:	in tectonic fabrics: WmI+Ampl+GrtI +Rt±Ompl	not found	in tectonic fabrics: WmI+GrtI+CldI +Ky+Rt+Tur
<b>stage 1</b> crenulation	WmII/III+Qtz+GrtII +Ompl/II+Ampl+Ky+Rt	not found	not found	not found
<b>D2</b>	in tectonic and mylonitic fabrics:	in all fabrics:	not found	in tectonic fabrics:
		WmI+Ampl/II+GrtI+Rt ±Ompl/II±Zo±Cc	in all fabrics: WmII+Ampl+GrtI+Rt ±Ompl±Zo/Czo±Cc	WmI+GrtI+Rt +Ky+CldI±Cc+Tur
<b>stage 2</b> crenulation cleavage				
<b>stage 3</b> complete S <sub>2</sub> development	WmII/III+Qtz+GrtII +Ompl/II+Ampl+Rt			
<b>D3</b>		not found	not found	not found
<b>D4</b>	in shear zones: WmIV+Qtz+Czol Gln+GrtII+Ttn	in coronitic fabrics: WmII+AmplIII +Czol+GrtI+Ttn±Qtz	in shear zones: WmIII+AmplII+GrtI+Ttn ±Czol+Qtz	not found
<b>D5</b>	in coronitic and tectonic fabrics: WmV+Fe-Chl+Ab+ Act+Qtz+Czol+Ttn	in coronitic and tectonic fabrics: WmIII+Act+Ab +Czol+Chl+Ttn±Qtz	in coronitic and tectonic fabrics: WmIV+Act+Ab+Ttn +CzolIII+Qtz+Chl	in tectonic fabrics: WmII+CldII±Cc +Cc+Chl
<b>D6</b>	no new metamorphic minerals	no new metamorphic minerals	no new metamorphic minerals	no new metamorphic minerals

Fig. 6 Microphotographs show relationships between microstructural evolution and mineral growth during pre-D<sub>1</sub>, D<sub>1</sub> and D<sub>2</sub> deformation phases. **(A)** Red-brown Bt and Sil are concentrated in thin-films, defining the pre-Alpine foliation. Pl-sites are completely replaced by Omp and WmII fine-grained aggregates. Ky completely replaced the Sil sites; plane polarized light, base of photo = 3 mm. **(B)** Rt-rich core of pre-Alpine Amp within an Amp-bearing eclogite. Smaller grains of AmpI, and WmI constitute the rims; plane polarised light, base of photo = 0.75 mm. **(C)** S<sub>1</sub> foliation of an Amp-bearing micaschist, marked by SPO of AmpI, WmII and Qtz, microfolded during D<sub>2</sub>. S<sub>2</sub> crenulation cleavage is marked by SPO of small strain free AmpII and reoriented WmII. Grt has large Wm grains as inclusions both within the microlithons and the microfilms; crossed polarisers, base of photo = 2 mm. **(D)** D<sub>2</sub> fold hinges within glaucophanites. S<sub>1</sub>, marked by SPO of AmpI and WmI, is folded during D<sub>2</sub>; newly re-crystallised AmpII and WmII grains and re-oriented AmpI and WmI grains define the S<sub>2</sub> foliation; crossed polarisers, base of photo = 1.5 mm. **(E)** OmpI showing the "rosette texture". S<sub>2</sub> marked by SPO of WmII, Zo and AmpII, wraps around OmpI grain; plane polarised light, base of photo = 2 mm. **(F)** S<sub>2</sub> continuous foliation is marked by SPO of OmpII and WmIII grains. WmIII is slightly deformed, showing undulose extinction, during D<sub>6</sub> deformation phase. GrtII boundaries are rational with respect to WmIII and OmII grains; plane polarised light, base of photo = 3 mm. **(G)** S<sub>2</sub> in amphibole bearing eclogites: AmpI SPO defines the S<sub>2</sub> foliation; large GrtI porphyroblast contain AmpI grains smaller than those marking S<sub>2</sub> within the matrix. Within the central Grt porphyroblast the internal foliation is marked by SPO of the smaller AmpI grains and is gently bent with respect to the external S<sub>2</sub> foliation; crossed polarisers, base of photo = 2.5 mm. **(H)** S<sub>2</sub> marked by SPO of Wm, Omp, Zo and Grt-rich bands within meta-quartzdiorites; plane polarized light, base of photo = 2 mm.



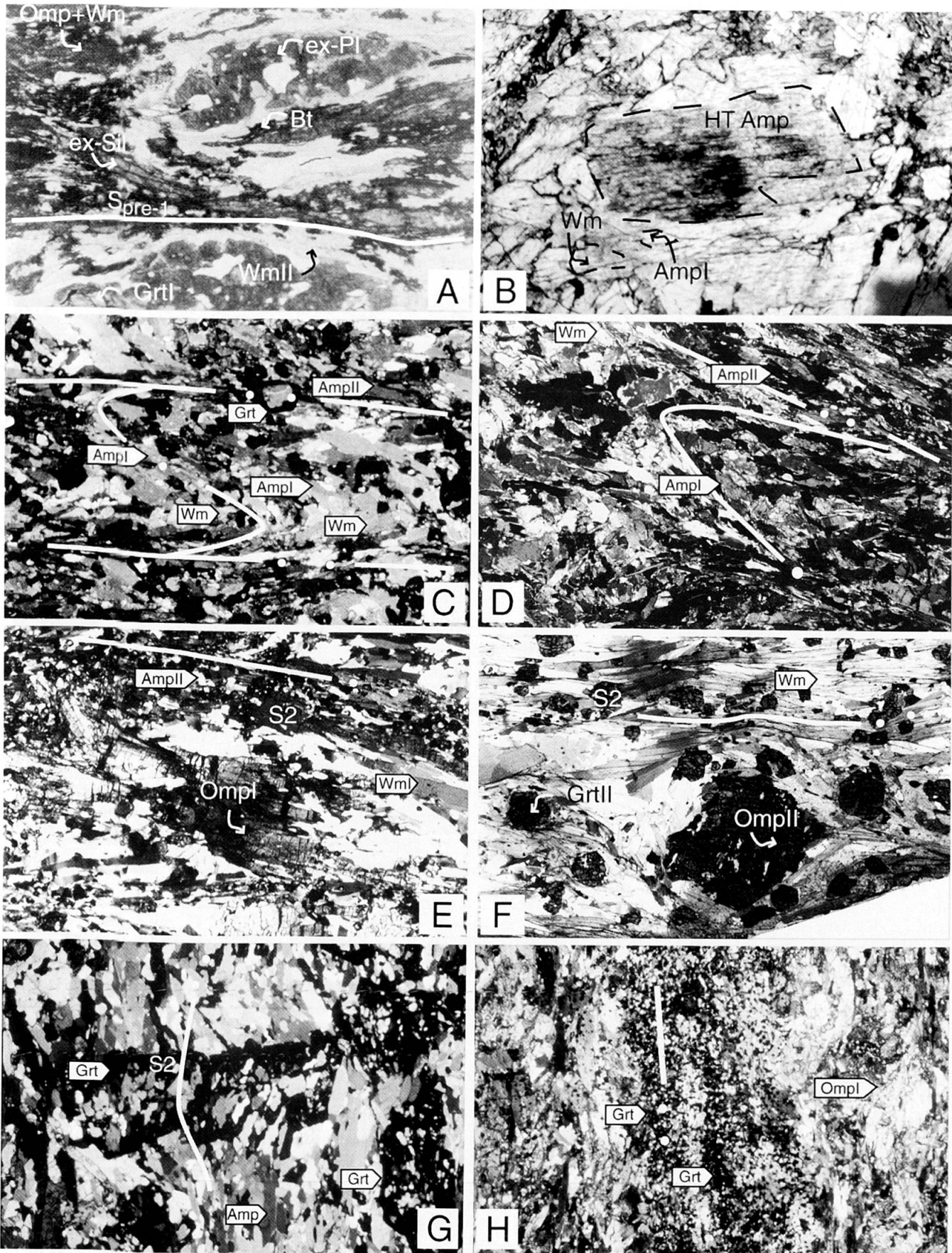
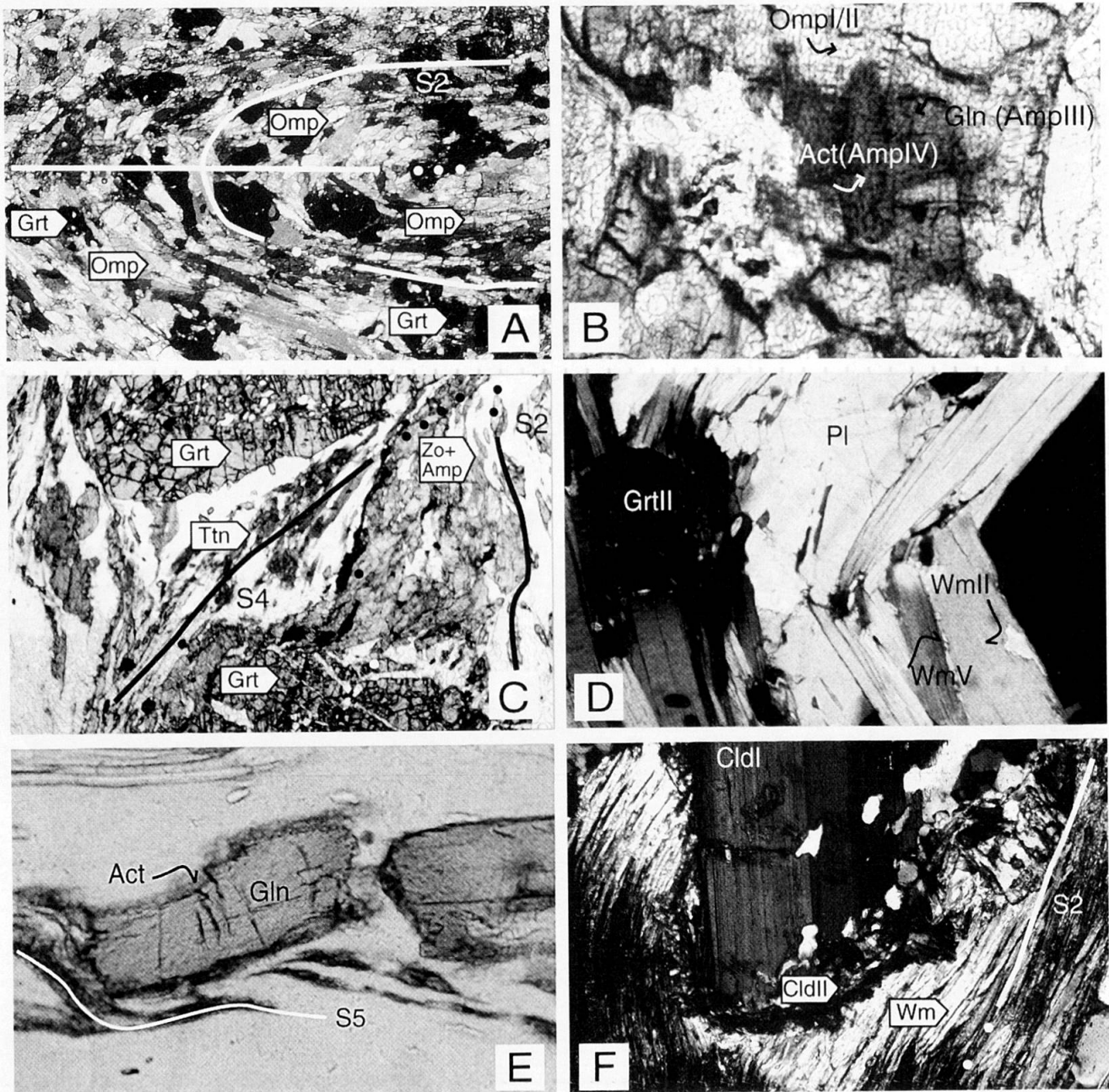


Fig. 6





*Fig. 7* Microphotographs show relationships between microstructural evolution and mineral growth during  $D_3$ ,  $D_4$  and  $D_5$  deformation phases. **(A)**  $S_2$  marked by SPO of OmpI/II, WmII and AmpII, bent by  $D_3$  microfold. WmII and GlnII show undulose extinction; GrtII, OmpI, AmpII and WmII boundaries are rational; crossed polarisers, base of photo = 1.5 mm. **(B)** Neck of fractured OmpI/II filled by AmpIII during  $D_4$  and by Act during  $D_5$ ; plane polarisers, base of photo = 0.50 mm. **(C)** Syn- $D_4$  microshear band, between two Grt porphyroblasts, defined by SPO of AmpIII, Czo and Ttn; plane polarised light, base of photo = 2.50 mm. **(D)**  $D_5$  microfold in micaschist; saddle reef triangular domain is filled by strain free Ab, while Wm grains are sutured and show undulose extinction and deformation bands. Small grained Wm fills the (001) planes and the grain boundaries; thin Chl occupies garnet-white mica grain boundaries; crossed polarisers, base of photo = 0.75 mm. **(E)**  $D_5$  micro-fracturing of Gln with SPO parallel to  $S_2$ ; green-Amp aggregates fill the boudin neck and are aligned parallel to  $S_5$ ; plane polarised light, base of photo = 0.50 mm. **(F)** Small grains of CldII rim the large CldI porphyroblast within the Grt-Cld-Ky-bearing quartzites at Balmenegre-Druer. The CldI is wrapped by a WmI stacks, which mark the  $S_2$  crenulation cleavage. CldI shows polysynthetic twinning and a few quartz inclusions. An aggregate of thin grained WmII developed at boundaries between WmI and CldII; crossed polarisers, length of photo = 0.75 mm.

In the low strain domains of meta-quartzdiorites a heterogranular igneous texture is preserved, but the igneous mineral assemblage is completely replaced.

Pl microstructural sites are overgrown by Cpx aggregates or porphyroblasts; Amp cores rich in Rt inclusions suggest the occurrence of pristine Ti-rich Amp.

In metabasites no pre-Alpine fabrics have been recognised and the only pre-D<sub>1</sub> relics are brown Hbl cores of Amp (Fig. 6b).

#### 4.2. ALPINE ECLOGITIC EVOLUTION

**Syn-D<sub>1</sub>** S<sub>1</sub> is preserved only in metapelites, metabasites, and quartzites. Eclogite facies minerals define the S<sub>1</sub> foliation in all lithologies (Fig. 8 and Table 3).

In *metapelites* S<sub>1</sub> is a spaced foliation marked by SPO of WmII, AmpI ± OmpI, locally coinciding with GrtII bands, whereas microlithons contain Qtz, GrtII, Rt and WmII porphyroblasts. Boundaries between GrtII and WmII are rational surface of either phase. Rt and GrtII within lithons occur as isolated grains, bands or as inclusions within WmII, AmpI and OmpI.

In small volumes of mica-rich *glaucophanites* the relic foliation S<sub>1</sub> is marked by a SPO of large AmpI, and WmI grains (Fig. 6d) associated with Rt. AmpI shows undulose extinction, deformation bands and sub-grains. GrtI porphyroblasts show an internal foliation (Si), marked by gently bent AmpI grains smaller than in the matrix, suggesting garnet growth during an earlier stage of Se (S<sub>1</sub>).

S<sub>1</sub> foliation in *quartzites* is relict within S<sub>2</sub> microlithons and is marked by a SPO of WmI large porphyroblasts showing undulose extinction and deformation bands.

**Syn-D<sub>2</sub> (stage 1)** Stage 1 of S<sub>2</sub> development is only recorded in metapelites and corresponds to crenulation of S<sub>1</sub> (Fig. 8).

Within D<sub>2</sub> micro-hinges AmpI, OmpI and WmII are bent and display undulose extinction and deformation bands.

**Syn-D<sub>2</sub> (stage 2)** During stage 2 the S<sub>2</sub> axial plane foliation develops. Stage 2 is well recorded in metapelites (Figs. 6c–8), in metabasites (Figs. 6d–8) and in quartzites (Fig. 8). Eclogite facies assemblages mark the S<sub>2</sub> foliation in all lithologies (Fig. 8 and Table 3).

In *metapelites* S<sub>2</sub> is a crenulation cleavage marked by SPO of AmpI, WmII (Fig. 6c) and OmpI. SPO of the smaller undeformed new grains of AmpII and WmIII defines S<sub>2</sub>. GrtII occurs within thinfilms and microlithons and forms rational boundaries with WmII and AmpI lying on S<sub>2</sub>. OmpI grains show undulose extinction, deformation bands and sub-grains (Fig. 6e). The formation of OmpII stack may result from recrystallisation of OmpI, as proposed for amphibole by BIERMANN (1977). WmII shows undulose extinction and deformation bands. Qtz, within Q domains, commonly shows undulose extinction, deformation bands and sub-grains parallel to S<sub>2</sub>.

WmII, AmpI porphyroclasts, showing undulose extinction define S<sub>2</sub> in *metabasites* (Fig. 6d); smaller strain-free AmpII develops as new grains at AmpI rims or un-

derline S<sub>2</sub>; large GrtI porphyroblasts occur within S<sub>2</sub> microlithons.

S<sub>2</sub> in *quartzites* is characterised by a crenulation cleavage (Fig. 8) marked by CldI, WmII, Ky and Qtz. GrtI, CldI, and bent WmI occur into rootless fold hinges and in S<sub>2</sub> lithons.

**Syn-D<sub>2</sub> (stage 3)** At this stage S<sub>2</sub> is a continuous foliation in all lithologies (Fig. 6 and 8) and the structural and mineralogical re-equilibration is complete.

In *metapelite* S<sub>2</sub> is a continuous foliation marked by SPO of WmIII, AmpII, OmpII and Rt (Fig. 6f). OmpII and AmpII grains are strain-free and no reaction rims occur between the two phases, suggesting Omp and Amp are stable during this stage of S<sub>2</sub> development.

In *eclogite* S<sub>2</sub> is marked by SPO of small strain-free OmpII and AmpII grains associated with GrtI and minor WmI. Rt occurs as inclusions within OmpI and AmpI porphyroclasts, re-oriented in S<sub>2</sub>, or as isolated grains.

In *meta-quartzdiorite* S<sub>2</sub> is marked by SPO of ZoI + Qtz + WmII ± AmpI ± Rt associated with GrtI-rich layers, Ap and Zr (Fig. 6h). WmII have (001) planes mainly parallel to S<sub>2</sub> and in place Rt inclusions along (001) occur. OmpI are mainly large porphyroblasts rich in Rt and AmpI inclusions, without a preferred orientation; OmpI shows rational boundaries with WmII, ZoI, AmpI and GrtI.

Large GrtI net-fish porphyroblasts rich in CldI random inclusions occupy S<sub>2</sub> lithons in *quartzite*. Zoned CldI shows polysynthetic twinning parallel to the S<sub>2</sub> foliation (Fig. 7f). Ky porphyroblasts, rich in Rt inclusions, occur in S<sub>2</sub> microlithons with SPO parallel to S<sub>2</sub>. Zoned Tur is enclosed within garnet porphyroblasts or occur in S<sub>2</sub> Qtz-rich domains.

The inferred stable assemblages during D<sub>1</sub> and D<sub>2</sub> deformations are summarized in Table 3.

**Syn-D<sub>3</sub>** The D<sub>3</sub> deformation phase has been recognised in metapelite only. It consists of a crenulation of pre-existing foliations (Fig. 7a).

Omp, Amp and Wm grains, bent within D<sub>3</sub> fold hinges are characterized by deformation bands and sub-grains.

The inferred stable assemblage during D<sub>3</sub> in *metapelites* is reported in Table 3.

**Syn-eclogitic coronitic textures** The undeformed lozenge, containing pre-Alpine relict textures show a pervasive eclogite facies re-equilibration that cannot be unequivocally related to D<sub>1</sub>, D<sub>2</sub> or D<sub>3</sub>. These domains only occur in metapelite and meta-quartzdiorite.

Where *metapelite* still preserves pre-D<sub>1</sub> fabrics and corresponding mineralogical assemblages, WmII, GrtII and opaque minerals grow as coronas of Bt; WmI is partially replaced by fine-grained WmII and it is rimmed by small GrtII. OmpI aggregates and fine-grained WmII completely overgrown Pl; OmpI and small GrtII rim GrtI; Ky aggregates replace Sil.

In *meta-quartzdiorite* coronitic domains, the eclogit-



ic assemblage, WmII+Zo/CzoI+Qtz + AmpI±OmpI, completely replaced the igneous minerals.

#### 4.3. ALPINE RETROGRESSION

**Syn-D<sub>4</sub>** During D<sub>4</sub> micro-fracturing (Fig. 7b), micro-boudinage and a S<sub>4</sub> discontinuous foliation or shear bands (Fig. 7c) develop. Epidote-blue-schist facies assemblages define D<sub>4</sub> fabrics in all lithologies (Table 3).

In *metapelite* during D<sub>4</sub> OmpI/II is partially replaced by AmpIII (Gln) within boudin and fracture necks (Fig. 7b). AmpIII also defines coronas of OmpI/II. Ttn occurs as coronas around Rt grains. SPO of AmpIII, CzoI, Qtz, Ttn and thin-grained WmIV define microshear zones, which deflected the previous foliations. AmpIII, GrtII and CzoI have rational boundaries.

In *metabasite* SPO of AmpIII, WmII and CzoI defines S<sub>4</sub>. AmpIII grains are small strain free, with rational boundaries with respect to adjacent WmII, CzoI and GrtI. WmII shows slight undulose extinction and rational boundaries. AmpIII fills fractures and boudins of OmpI/II and AmpI/II. Ttn defines coronas over Rt.

In *meta-quartzdiorite* S<sub>4</sub> forms discrete shear bands defined by SPO of AmpII (Gln) + CzoII, WmIII aggregates and Ttn. S<sub>4</sub> deflects the S<sub>2</sub> foliation and is locally associated with boudinage of OmpI and AmpI. AmpII, CzoII and GrtI show rational boundaries. The same minerals replace the eclogitic assemblage in coronitic domains: AmpII rims AmpI and OmpI grains, CzoII replaces ZoI or occurs as isolated newly crystallised grains; Ttn rims Rt.

The inferred syn-D<sub>4</sub> stable assemblage is reported in Table 3.

**Syn-D<sub>5</sub>** D<sub>5</sub> structures are mainly characterized by micro-folding (Fig. 7d) of pre-existing foliations and folds (Fig. 8). D<sub>5</sub> is only locally associated to the development of a foliation (S<sub>5</sub>), defined by greenschist facies assemblages (Fig. 7e). Syn-D<sub>5</sub> transformations within metabasites only occur as coronas (Fig. 8).

In *metapelite* D<sub>5</sub> is locally associated with a foliation (S<sub>5</sub>) defined by SPO of Chl, Ab, Act, CzoII, Ttn and WmV. Within D<sub>5</sub> fold hinges, Qtz is elongate and shows undulose extinction, indented boundaries and SPO parallel to the D<sub>5</sub> fold axial planes. Small strain-free grains of CzoII occupy the D<sub>5</sub> fold hinges and show rational boundaries with WmIII kinked grains. WmV new grains develop along (001) planes of kinked WmIII. Fe-Chl and Ab-rich Pl fill WmII saddle reefs (Fig. 7d) or GrtII cracks and replace OmpI/II, AmpI/II and WmII/III. Act partially replaces AmpI/II re-oriented porphyroclasts.

In *metabasite* Act rims AmpI/II, fills AmpI/II micro-fractures or occurs as green needles. Chl partially replaces GrtI, AmpI/II, OmpI/II and WmI/II. Ttn rims Rt.

S<sub>5</sub> in *meta-quartzdiorite* is marked by fine-grained

Act, Chl and WmIV or by SPO of CzoIII and Ab. Ab and Act replaces OmpI and AmpI grains. Ab also replaces WmII. CzoIII, Ttn and Ab occupy D<sub>5</sub> lithons. Chl replaces GrtI; Ttn rims Rt and CzoIII rims Zo/CzoI and CzoII.

Within *quartzite* fold hinges large WmI grains are rimmed by fine-grained WmII aggregates associated with CldII and ChlI. Small CldII aggregates rim CldI porphyroblasts within D<sub>5</sub> lithons (Fig. 7f).

For inferred stable assemblages see Table 3.

**Syn-D<sub>6</sub>** D<sub>6</sub> deformation is not associated with metamorphic transformation and only slightly influences the microstructure. It is mainly characterized by gentle crenulation of pre-existing foliations and minerals (e.g. Wm, Czo, Act and Chl).

### 5. Mineral Composition

Minerals were analysed with an ARL-SEMO electron microprobe and natural silicates were used as standards; matrix corrections were calculated with ZAF procedure. The accelerating voltage was 15kV, the sample current 20 nA and beam current 300 nA. Representative mineral compositions from metapelite, quartzite, meta-intrusives and metabasites are shown in the Appendix.

*Amphiboles* syn-kinematic with stage 3 of the S<sub>2</sub> development, syn-D<sub>4</sub> and syn-D<sub>5</sub> were analysed (Figs. 9a-b). They are mainly barroisites, actinolitic hornblendes and actinolites with minor glaucophanes. AmpI and AmpII have barroisitic composition, AmpIII is Gln and Act-hornblende and syn-D<sub>5</sub> amphibole show mainly Act compositions. *Garnets* show a homogeneous composition in different rocks (Fig. 9c and Appendix) and plot in the "Group C eclogites" field according to COLEMAN (1965). Syn-D<sub>1</sub>, D<sub>2</sub>, D<sub>3</sub>, D<sub>4</sub> and D<sub>5</sub> *white micas* were analysed in metapelites, meta-quartzdiorites and quartzites; they have phengitic and paragonitic compositions. Phengitic micas show variable amounts of celadonic substitution depending on the microstructural site (Fig. 9d and Appendix). A strong Mg depletion marks the compositional evolution from *CldI* and *CldII* (Appendix and Fig. 9e). *Clinopyroxenes* were analysed in metagranitoids and metapelites: OmpI and OmpII in metapelites show no difference in their composition, while Omp in metagranitoids shows compositional variations from core to rim (Appendix and Fig. 9f). In metapelites and meta-quartzdiorites, syn-D<sub>2</sub> *epidote* group minerals are Zo and Czo, while syn-D<sub>4</sub> and syn-D<sub>5</sub> show the highest 'Al<sub>2</sub>Fe' values (Appendix). *Chlorite* in metabasites and meta-quartzdiorites has  $0.55 \leq X_{Mg} \leq 0.65$  and in quartzites  $0.24 \leq X_{Mg} \leq 0.40$ . Syn-D<sub>5</sub> *plagioclase* is Ab (Na = 0.90–0.97 a.p.f.u.).

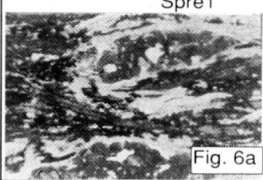
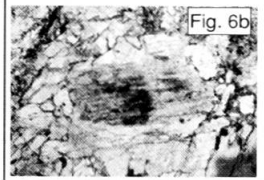
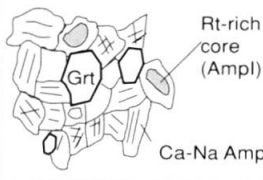

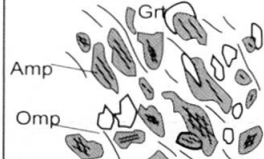
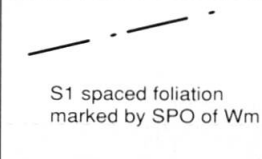
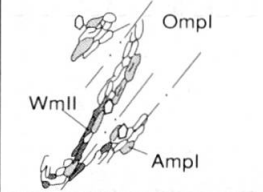
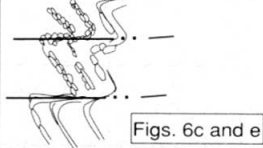
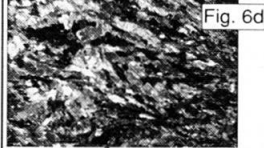

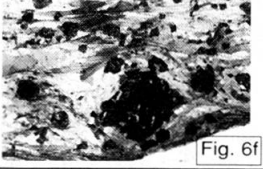
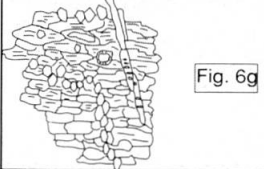
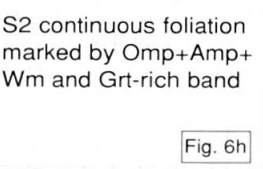
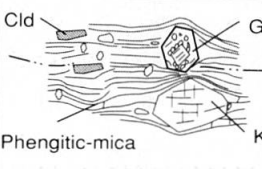
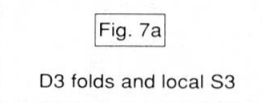
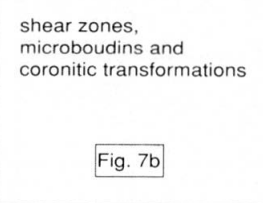
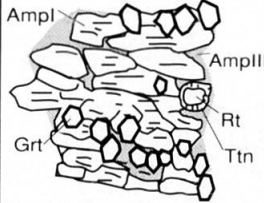
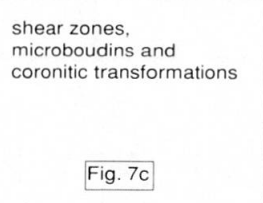
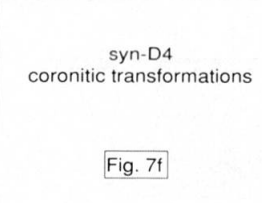
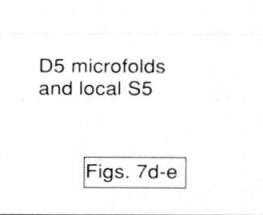
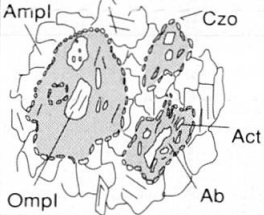
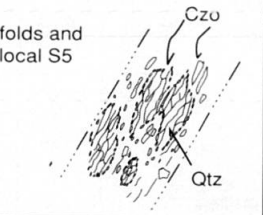
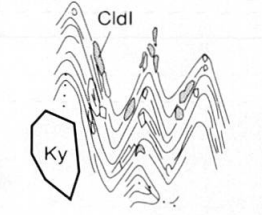

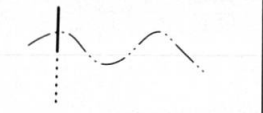

Deformation phases	Metapelites	Metabasites	Meta-intrusives	Cld-Ky-Grt quartzites
<b>pre-D1</b>				not found
<b>D1</b>			not found	
<b>stage 1</b> crenulation		not found	not found	not found
<b>D2 stage 2</b> crenulation cleavage			not found	
<b>stage 3</b> complete S2 development			S2 continuous foliation marked by Omp+Amp+Wm and Grt-rich band 	
<b>D3</b>		not found or coronitic transformations	not found or coronitic transformations	not found or coronitic transformations
<b>D4</b>	shear zones, microboudins and coronitic transformations 		shear zones, microboudins and coronitic transformations 	syn-D4 coronitic transformations 
<b>D5</b>	D5 microfolds and local S5 		folds and local S5 	
<b>D6</b>		not found		

Fig. 8 Synoptic representation of microstructural evolutions during successive deformation phases in metapelites, metaintrusives, metabasites and Cld-Ky-Grt bearing quartzites. Stages 1, 2 and 3 have been distinguished within D<sub>2</sub> deformation phase on the basis of microstructural analysis. Labels link sketches with photomicrographs in Fig. 6 and 7.



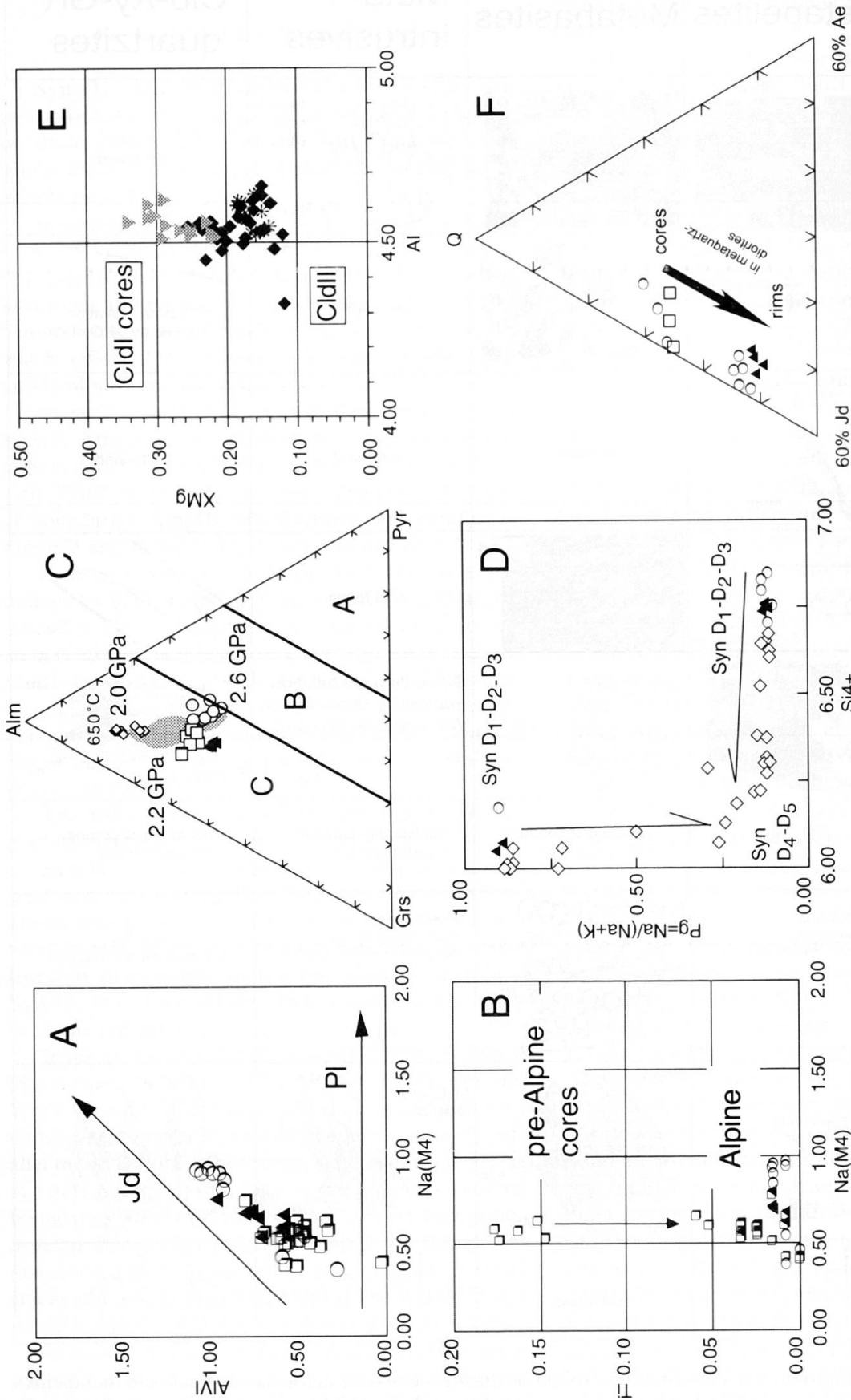


Fig. 9 (A) Diagram showing the significant substitutions in the amphiboles from metagranitoids (open circles), metapelites (black triangles) and metabasites (open squares). Jd and Pl represent the jadeite and plagioclase vectors. (B) Ti vs. Na(M4) content variations from pre-Alpine to Alpine amphiboles. Symbols as in a. (C) Garnet compositions for meta-quartzdiorites, metapelites, metabasites (symbols as in A) and quartzites (open diamonds). A, B and C are the fields in which plot garnet from different eclogite types according to COLEMAN (1965). Large shaded ellipses correspond to the composition of garnet synthesized in basaltic system at 650°C and 2.0–2.2–2.6 GPa by POLI (1993). (D) White mica compositions from quartzites, metapelites and meta-quartzdiorites (symbols as in a and C). Syn-D<sub>1</sub>-D<sub>2</sub>-D<sub>3</sub> white micas are characterised by high Si<sup>4+</sup> and high Pg. The syn-D<sub>4</sub>-D<sub>5</sub> grains show low Si<sup>4+</sup> and low Pg-contents (symbols as in c). (E) Chloritoid compositions from ky-clid-grt-bearing quartzites at Balmenegre-Druer. CldI cores (grey downward triangles) show highest values of X<sub>Mg</sub>; CldII (black diamonds) new grains and CldI (asterisks) rims show a decrease in X<sub>Mg</sub>. Al varies from 1.93 and 2.06 a.p.f.u. (F) Pyroxene compositions plotted into the Na-pyroxene triangular representation, after MORIMOTO (1988).

## 6. Metamorphic history

Mineral assemblages stable during the superposed deformations events were used together with thermobarometrical estimates to define the physical conditions of the metamorphic evolution.

Since most of the rocks show disequilibrium textures, in response to successive structural and metamorphic overprints, thermobarometry was applied only to mineral pairs in mutual contact with clean grain boundaries. Results of thermobarometry are reported in Table 4 and Fig. 10. Pressure and temperature stability fields of metamorphic assemblages or reaction equilibria were calculated using Thermocalc (HOLLAND and POWELL, 1990) and Perplex (CONNOLLY, 1990). Activities for Thermocalc calculations were obtained using Ax (HOLLAND and POWELL, 2000).

### 6.1. PRE-ALPINE EVOLUTION

Temperatures of  $720 \pm 48$  °C and minimum pressures of  $0.3 \pm 0.05$  GPa were obtained applying thermobarometers on pre-Alpine Amp cores in metabasites (Table 4), where the lack of pre-Alpine Grt allows the use of the empirical barometer based on the  $Al^{tot}$  content of Amp (HAMMARSTROM and ZEN, 1986; HOLLISTER et al. 1987; JOHNSON and RUTHERFORD, 1989). This estimated P-T interval is compatible with the occurrence of  $D_{pre-1}$  pre-Alpine assemblage Grt + Bt + Sil + Pl + Qtz + Ilm  $\pm$  Kfs  $\pm$  Wm preserved in metre-size undeformed lenses within eclogitised metapelites (e.g. THOMPSON, 1976; SPEAR, 1993).

### 6.2. ALPINE HP EVOLUTION

Several thermobarometers were applied to syn- $D_2$  mineral pairs in metapelites, quartzites, meta-quartzdiorites and metabasites (Table 4). Estimated P-T conditions are reported in Fig. 10 and Table 4. Pressures obtained with the barometer based on  $Si^{4+}$  contents in phengitic mica (MASONNE and SCHREYER, 1987) indicates  $P > 1.0$ – $1.1$  GPa for the estimated interval of 500–600 °C (Table 4). The barometer based on the Jd content in Omp (HOLLAND, 1980) yields pressure of  $1.3 \pm 0.2$  GPa for the same temperature interval. Chemical compositions of syn- $D_2$  amphiboles and garnet were compared with amphiboles synthesized in HP experimental studies on tonalitic and basaltic compositions at 550–650 °C (SCHMIDT, 1993; POLI, 1993). Compositions of the analysed amphiboles are compatible with P of 1.6–1.8 GPa, whereas Mg contents within GrtI are similar to garnet synthesized in the P-range of 2.2–2.6 GPa at  $T = 650$  °C.

P estimates derived by classical barometers are markedly lower than P-values suggested by amphibole and garnet compositions; Jd content in clinopyroxene and  $Si^{4+}$  content in white mica are buffered by the bulk composition and should therefore indicate minimum pressures. The occurrence of the Omp + Grt  $\pm$  Zo  $\pm$  Amp + Wm + Qtz metamorphic association in metapelites (Fig. 10) yields minimum pressures of 1.5–1.8 GPa for this temperature range (using Perplex; CONNOLLY, 1990). In quartzites the divariant equilibrium Cld = Grt + Ky (Fig. 10) indicates minimum P of 1.5–2.1 GPa, whereas the univariant equilibrium Omp + Grt + Q = Zo + Bar demands  $P \geq 1.5$  GPa at  $T \leq 600$  °C. Up to now, Coesite has not been described from the entire Sesia-Lanzo Zone; this suggests that the maximum P-values may be below the univariant equilibrium Coe = Qtz (Fig. 10; BOHLEN and BOETTCHER, 1982).

### 6.3. ALPINE RETROGRESSION

During  $D_4$  deformation the assemblage Czo + Gln + Ttn  $\pm$  Grt developed at the expense of Omp + Grt in metapelites, meta-quartzdiorites, and metabasites. This indicates that during  $D_4$  re-equilibration reached  $P \leq 1.5$  GPa and  $T \leq 500$ , as suggested by the univariant equilibria Omp + Rt + Qtz +  $H_2O$  = Ttn + Gln and Omp + Grt +  $H_2O$  = Gln + Czo (Fig. 10) calculated using Thermocalc (HOLLAND and POWELL, 1990). The widespread occurrence of Ttn coronas around Rt grains and the Omp break-down in metabasites indicate a syn- $D_4$  pressure decrease, when the experimental data obtained by LIOU et al. (1998) on MORB +  $H_2O$  system and by POLI (1993) and SCHMIDT (1993) on basaltic and tonalitic systems are taken into account.

Syn- $D_5$  assemblages could be explained by the reactions Czo + Gln + Qtz +  $H_2O$  = Tr + Chl + Ab (MARUYAMA et al., 1986) and Grt + Czo + Qtz +  $H_2O$  = Act + Chl (HOLLAND and POWELL, 1990). The two univariant equilibria indicate that  $T \leq 330$  °C and  $P \leq 0.7$  GPa were attained during that deformation stage. This P-retrograde evolution, taking place during  $D_4$  and  $D_5$  deformations, is also recorded by the  $X_{Mg}$  decrease from CldI (syn- $D_2$ ) to CldII (syn- $D_5$ ) in quartzite.

## 7. Strain partitioning, degree of fabric evolution and metamorphic transformation

In this portion of the EMC of the SLZ seven phases of deformation have been identified, each of them characterised by coexisting heterogeneous strain states (coronitic, tectonic and mylonitic).

ic domains). The evolving mineral assemblages shown suggest successive re-equilibration under changing pressure and temperature conditions. However, the degree to which new metamorphic assemblages grew, i.e. the metamorphic imprint, is

highly heterogeneous. The degree of fabric evolution and of metamorphic imprint do not necessarily correspond in adjacent rock volumes (Fig. 11), i.e. the degree of deformational imprint (e.g.  $D_2$  and  $D_5$  folds and granular scale deformation)

Table 4 Pre-Alpine and Alpine thermobarometric estimates for metapelites, metabasites, Ky-Cld-Grt quartzites, meta-quartzdiorites and eclogites.

Calibration	T(°C)	P(GPa)	References
<b>Pre-Alpine evolution</b>			
<i>metabasites</i>			
Ti in Amp	720±48		OTTEN, 1984
Al in Amp		0.3±0.05	HAMMARSTROM and ZEN, 1986; JOHNSON and RUTHERFORD, 1989
<b>Alpine HP evolution</b>			
<i>metapelites</i>			
OmpI-GrtII (Fe2-Mg)	545±15		POWELL and HOLLAND, 1985
OmpI-GrtII (Fe2-Mg)	520±15		KROGH, 1988
GrtII-WmII (Fe2-Mg)	510±40		HYNES and FOREST, 1988
Si4+ in WmII e WmIII		≥1.1	MASSONNE and SCHREYER, 1987
Jd in OmpI e OmpII		1.3±0.1	HOLLAND, 1980
Omp+Grt+Wm+Qtz±Zo±Amp	≤600	>1.5-1.8	calculated with Perplex (CONNOLLY, 1990)
<i>ky-cld-grt quartzites</i>			
GrtI-ctdI (Fe2-Mg)	575±20		PERCHUK, 1991
GrtI-turm (Fe2-Mg)	540-600		COLOPIETRO and FRIEBERG, 1987
GrtI-WmI (Fe2-Mg)	550±20		HYNES and FOREST, 1988
Si4+ in WmI		1.0	MASSONNE and SCHREYER, 1987
Cld=Grt+Ky	≤610	≥1.5	calculated with Perplex (CONNOLLY, 1990)
Cld=Ky+Grt+Chl	≤600		calculated with Perplex (CONNOLLY, 1990)
<i>metaquartzdiorites</i>			
OmpI-GrtI	550±50		POWELL and HOLLAND, 1985
"	520±50		KROGH, 1988
GrtI-WmI	520±20		HYNES and FOREST, 1988
Si4+ in WmI		1.0-1.2	MASSONNE and SCHREYER, 1987
Jd in OmpI		1.3±0.2	HOLLAND, 1980
Na(A) and Al <sub>tot</sub> in AmpI		1.6-1.8 or >2.0	SCHMIDT, 1993 (tonalitic system)
Ca, Na(M4) e Na <sub>tot</sub> in AmpI		1.6-1.8	SCHMIDT, 1993 (tonalitic system)
<i>metabasites</i>			
Na <sub>tot</sub>		1.6-1.8	POLI, 1993 (basaltic system)
X <sub>Mg</sub> in GrtI	650	2.2-2.6	POLI, 1993 (basaltic system)
Omp+Grt+Qtz=Zo/Czo+Bar	500-600	1.6-1.8	calculated with Perplex (CONNOLLY, 1990)
<i>Amp-bearing eclogites</i>			
Ti in Amp	560±10		OTTEN, 1984
GrtI-AmpI (Fe2-Mg)	500±80		PERCHUK, 1991
GrtI-AmpI (Fe2-Mg)	580±75		GRAHAM and POWELL, 1984
Grt-OmpI (Fe2-Mg)	550±20		POWELL and HOLLAND, 1985
Grt-OmpI (Fe2-Mg)	535±40		KROGH, 1988
Jd in OmpI		≥1.19	HOLLAND, 1980
<b>Alpine retrogression</b>			
<i>metapelites, metaquartzdiorites and metabasites</i>			
Omp+Rt+Qtz+H <sub>2</sub> O=Ttn+Gln	≤550	≤1.3	calculated with Thermocalc (HOLLAND and POWELL, 1990)
Omp+Grt+H <sub>2</sub> O=Gln+Czo	≤500	≤1.3	calculated with Thermocalc (HOLLAND and POWELL, 1990)
Czo+Gln+Qtz+H <sub>2</sub> O=Tr+Ab+Chl	≤500	≤0.8	MARUYAMA et al., 1986
Grt+Czo+Qtz+H <sub>2</sub> O=Act+Chl	≤320	≤0.75	HOLLAND and POWELL, 1990
<i>metabasites</i>			
Ttn replacing Rt		≤1.3	LIU, 1998

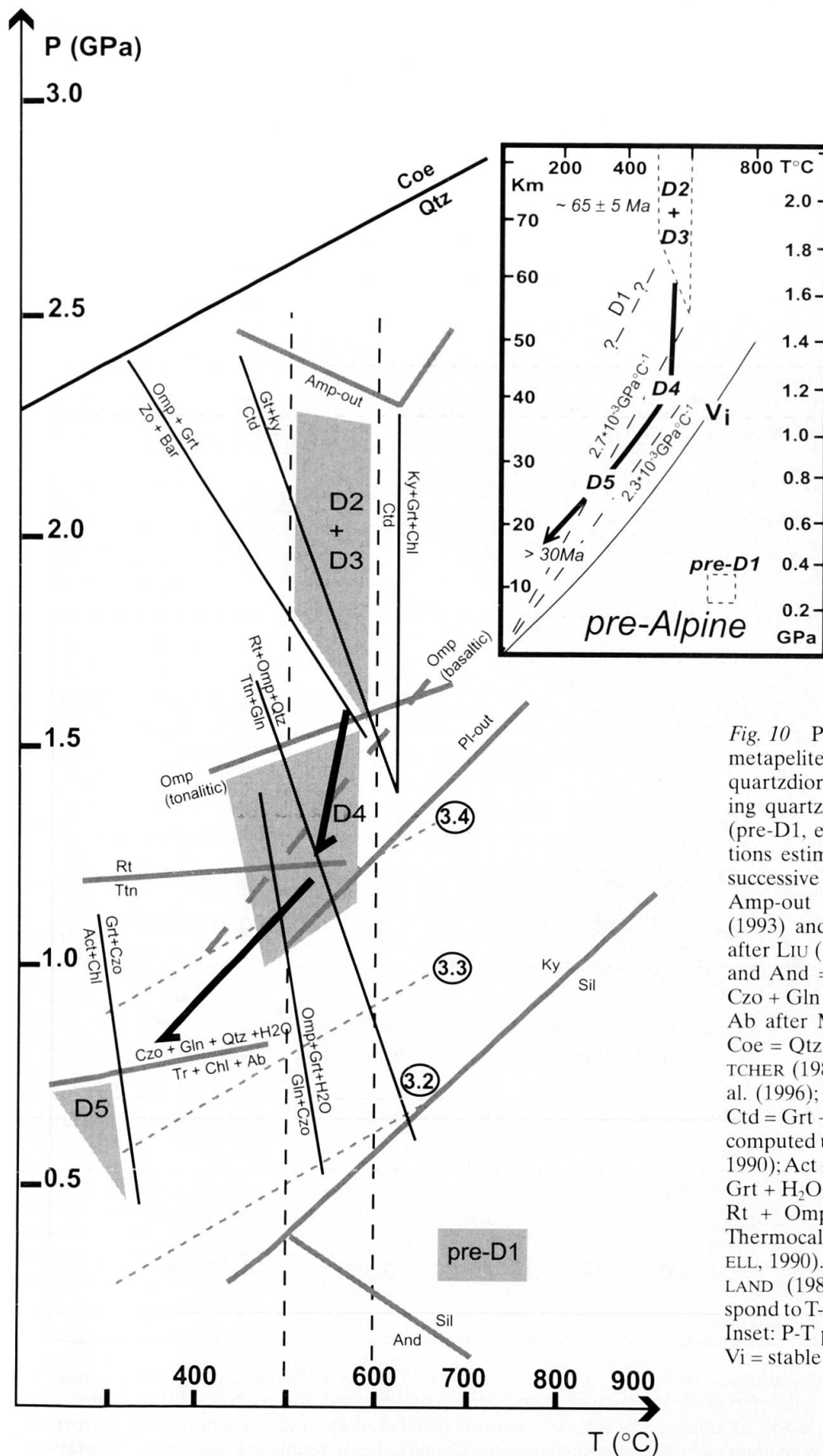


Fig. 10 P-T-d-t path inferred from metapelites, metabasites, meta-quartzdiorites and ky-grt-cld-bearing quartzites of EMC. Grey areas (pre-D1, etc.) represent P-T conditions estimated with respect to the successive deformation phases. Amp-out and Omp from POLI (1993) and SCHMIDT (1993); Pl-out after LIU (1996), Ky = Sil, And = Sill and And = Ky after SPEAR (1993); Czo + Gln + Qtz + H<sub>2</sub>O = Tr + Chl + Ab after MARUYAMA et al. (1986); Coe = Qtz after BOHLEN and BOETTCHER (1982); Rt = Ttn after LIU et al. (1996); Zo + Bar = Omp + Grt, Ctd = Grt + Ky, Ctd = Ky + Grt + Chl computed using Perplex (CONNOLLY, 1990); Act + Chl = Grt + Czo, Omp + Grt + H<sub>2</sub>O = Gln + Czo, Ttn + Gln = Rt + Omp + Qtz calculated with Thermocalc (HOLLAND and POWELL, 1990). Si<sup>4+</sup> isopleths after HOLLAND (1980). Vertical lines correspond to T-range reported in Table 3. Inset: P-T path of EMC of the SLZ. Vi = stable geotherm.



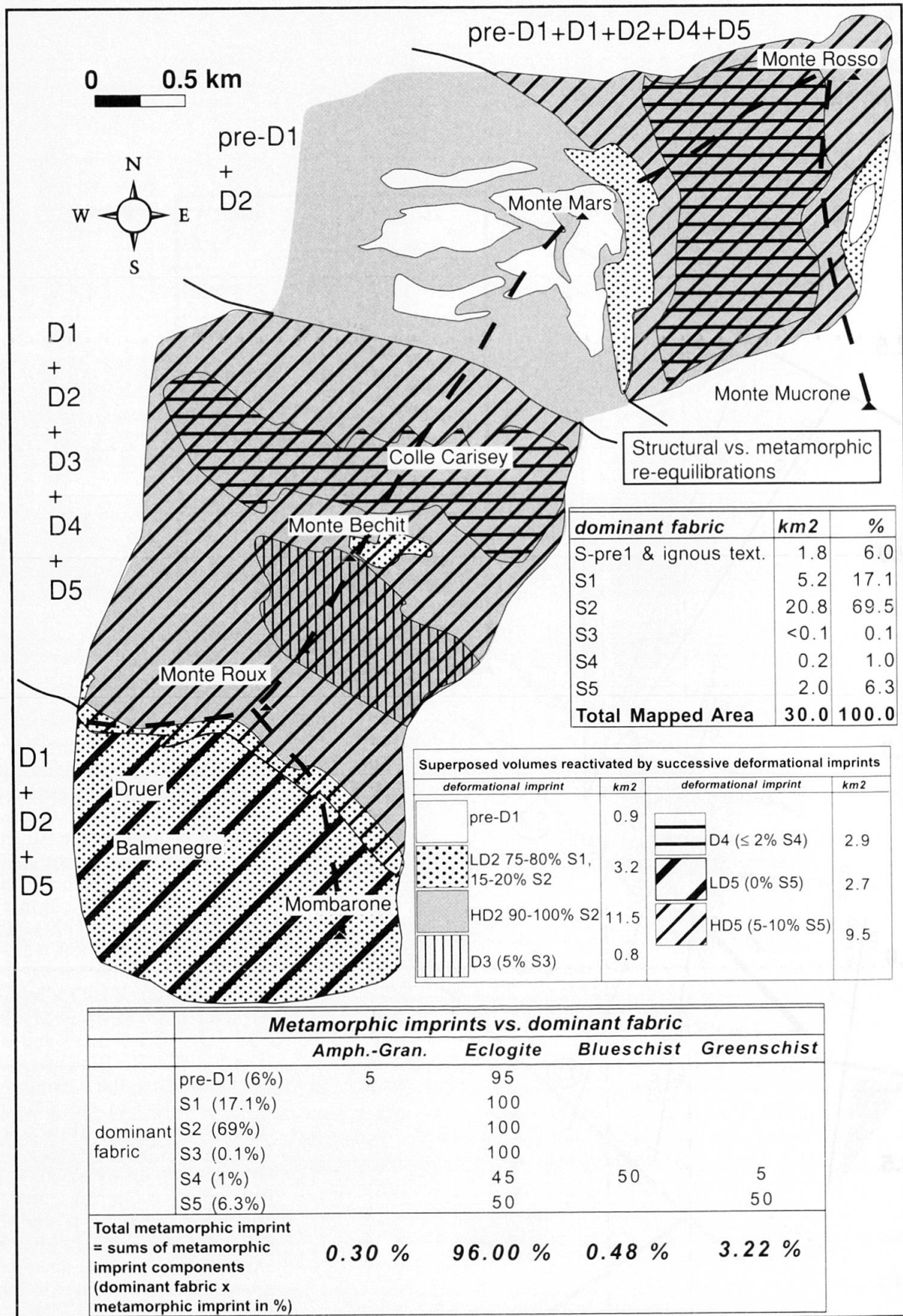


Fig. 11 Map of the superposition of successive phases of deformation (deformational imprint). At the map scale, domains characterised by the same relative timing of superposed structures are also contoured. The degree of new planar syn-metamorphic fabric (dominant fabric), the deformational imprint and metamorphic transformation (metamorphic imprint in percentage of syn-metamorphic minerals) have been quantified and reported in tables.

need not coincide with a corresponding degree of development of the syn-kinematic metamorphic transformation. In order to better illustrate and understand this heterogeneity at the map scale, we attempted to quantify separately the degree of fabric evolution and of metamorphic transformation. In Figure 11 the domains recording successive phases of deformation (deformational imprint), the areas in which a new syn-metamorphic fabric develops (dominant fabric) and the degree of metamorphic transformation (metamorphic imprint in percentage of syn-metamorphic minerals) are shown. Areas and percentages of deformational imprint and dominant fabric have been estimated on the basis of the original map; areas have been separately contoured and quantified using NiH image processor (RESBAND, 2001). The degree of metamorphic re-equilibration, which corresponds to the amount of new minerals, grown during each metamorphic stage (e.g. pre-Alpine and eclogitic), has been qualitatively estimated in thin section.

Figure 11 shows that the syn-eclogitic metamorphic and deformational imprint is the most spread in the area as well the syn- $D_1$  and  $D_2$  eclogitic fabrics ( $S_1$  and  $S_2$ ) are the dominant fabrics. This is in agreement with similar structural features observed within the EMC (e.g. GOSSO, 1977; WILLIAMS and COMPAGNONI, 1983). Figure 11 also shows that, where pre- $D_1$  fabrics are well preserved (100% of the area), the corresponding pre- $D_1$  mineral assemblages are scarce (compare Figs. 6a–b). In low grain-scale  $D_2$  deformation domains (= LD2) the  $S_1$  foliation occupies 75–80%, while  $S_2$  crenulation cleavage slightly overprints  $S_1$  (15–20%); the remaining areas may be occupied by successive fabrics (e.g.  $S_5$ ); in high grain-scale  $D_2$  deformation domains (= HD2) the  $S_2$  is penetrative (90–100%) and differentiated (stage 3 of the  $S_2$  development in Figs. 6–8).  $D_3$  domains are characterised by syn- $D_3$  folds, the  $S_3$  foliation is scarce ( $\leq 5\%$  in Fig. 11) and localized in fold hinges. In  $D_4$  areas metre-scale shear zones and  $S_4$  occupies  $\sim 2\%$  of  $D_4$  domains. Low grain-scale  $D_5$  deformation domains (= LD5) correspond to open folds without a new penetrative foliation, while in high grain-scale  $D_5$  deformation domains (= HD5) folds, from close to isoclinal in shape, are associated with a greenschist dominant fabric ( $S_5$ ), developing only within fold hinges (5–10% of LD5 domains). Figure 11 also shows that the degree of metamorphic imprint increases where the planar or linear fabric, syn-kinematic with each deformational imprint, is penetrative (dominant fabric). This positive correlation holds for syn- $D_4$  and  $D_5$  fabrics, but it does not exist for  $D_1$ ,  $D_2$  and  $D_3$  fabrics.

## 8. Conclusions

The tectono-metamorphic evolution may be summarised by a P-T-d-t path (Fig. 10), which indicates that the pre-Alpine (293 Ma) stage (pre- $D_1$ ) occurred at  $T = 720 \pm 48$  °C and  $P = 0.3 \pm 0.05$  GPa. During Alpine time ( $\sim 65$  Ma) meta-quartzdiorites of Monte Mars and Monte Mucrone, together with their surrounding rocks, were buried at depth  $\geq 55$  km ( $T = 500$ – $600$  °C and  $P \geq 1.5$  GPa for  $D_2$ ). The retrograde path is marked by a transition between blueschist facies conditions ( $D_4$  at  $T \leq 600$  °C and  $P \leq 1.5$  GPa) and greenschist facies conditions ( $D_5$  at  $T \leq 350$  °C and  $P \leq 0.7$  GPa), which ended before 30 Ma, as suggested by crosscutting relationships between  $D_5$  structures and Oligocene dykes. The pre-Alpine stage is characterised by a P/T ratio ( $0.4 \times 10^{-3}$  GPa/K) that corresponds to a very high T/depth ratio of  $\sim 70$  K/km. The Alpine eclogitic stage ( $D_2$ ) shows a P/T ratio ( $\geq 2.7 \times 10^{-3}$  GPa/K) corresponding to a T/depth ratio of  $\sim 10$  K/km. During the exhumation path ( $D_4$  and  $D_5$ , T/depth-ratio) is shifted towards higher values ( $\sim 14$  K/km) with a P/T ratio  $\geq 2.3 \times 10^{-3}$  GPa/K. The time interval between the eclogitic ( $D_2$ ) stage and the blueschist-greenschist exhumation ( $D_4$  and  $D_5$ ) conditions ( $\sim 35$  Ma) can be inferred from radiometric data available in the literature. The exhumation from the depth of  $\geq 55$  km (eclogitic peak) to the depth of  $\leq 20$  km (greenschist facies conditions) occurred under a very low thermal regime at an exhumation rate of  $\geq 1.4$  mm/year, if we consider the age of the Tertiary intrusive as a minimum age for the end of greenschist facies re-equilibration.

In addition, comparing the results of the present work (Fig. 11) with the deformational vs. metamorphic imprint schemes proposed for other portions of the EMC of the SLZ (Table 1), several conclusions can be drawn:

(1) During the Alpine evolution the heterogeneous structural and metamorphic imprint recorded in adjacent rock portions generated local variations in the relative deformation timing vs. metamorphic conditions showed in Table 1 and Fig. 11. Some heterogeneity may be related to specific major lithological variation. For example, at Monte Mars the large originally igneous body of meta-quartzdiorites constitutes a large volume that dominantly escaped the post  $D_2$  Alpine structural and metamorphic re-equilibration; at Mombarone the occurrence of a huge pre-Alpine marble-quartzite-micaschist multi-layer facilitated the diffuse memorisation of large scale  $D_2$  structures (Figs. 2–11), and the overprinting by successive structures was inhibited. In addition, domains displaying large-scale penetrative  $D_3$  structures were not diffusely affected by  $D_5$  isoclinal folding



and related metamorphic re-equilibration. Similar relationships between metamorphic overprint and deformation have been described for the SLZ by STÜNITZ (1989).

(2) Figure 11 shows a reconstruction of deformation vs. metamorphism relationships. The identification of a critical area is required before regional significance can be attributed to the correlation of structures, since the recorded deformation sequence changes across adjacent areas: e.g. in the Monte Mars region the prevailing deformation sequence corresponds to the pre- $D_1$  and  $D_2$  deformations; in the area of Monte Rosso the successive deformations are pre- $D_1$ ,  $D_1$ ,  $D_2$ ,  $D_4$  and  $D_5$ , while in the area of Monte Bechit-Monte Roux they are  $D_1$ ,  $D_2$ ,  $D_3$  and  $D_5$ .  $D_5$  structures (LD5 + HD5) affect the rocks to a large extent (Fig. 11); this locally corresponds to a new dominant fabric (~10%) where the pre-existing foliations ( $S_1$  and  $S_2$ ) are completely erased. Figure 11 also illustrates that in this area of ~30 km<sup>2</sup> the  $S_2$  foliation, marked by eclogite facies assemblages, is the dominant fabric and occupies ~60% of the area;  $D_4$  fabrics have only been recorded by a small proportion of rocks (~2%).

In addition, tables in Fig. 11 show the relationships between the dominant fabrics (complete structural re-equilibration) and corresponding metamorphic imprint: pre-Alpine fabric, well preserved in metre-size metapelites, corresponds to ~5% of pre-Alpine metamorphic assemblages and Alpine syn-eclogitic coronitic transformations defines the other 95%. In the examined slice ( $\geq 30$  km<sup>2</sup>) of continental crust involved in the Alpine very low T subduction/exhumation regime, the eclogite facies metamorphic imprint (syn- $D_1$ ,  $D_2$  and  $D_3$ ) affected  $\leq 96\%$  of the rocks, corresponding to 86.6% of complete syn-eclogitic structural re-equilibration (two penetrative foliations,  $S_1$  and  $S_2$ ). On the other hand, the scarce distribution of  $D_4$  and  $D_5$  planar and linear fabrics, with respect to the large distribution of syn- $D_5$  structures, corresponds to a low amount of intermediate P metamorphic imprints (3.7%). The scarce development of a new  $D_5$  fabric, in contrast with the penetrative  $D_2$  fabric, accounts for the large difference in volume percentage of eclogitic re-equilibration vs. greenschist re-equilibration. This conclusion is in agreement with observations from other Alpine areas (SPALLA et al., 2000) suggesting that the dominant metamorphic imprint is strongly influenced by the degree of fabric evolution.

#### Acknowledgements

The critical reading of Holger Stünitz and an anonymous reviewer greatly improved the paper. Useful and

fundamental suggestions of Martin Engi were providential. D. Biondelli provided assistance at the microprobe. G. Chiodi made microphotographs and C. Malinverno thin sections. The "CNR Centro di Studio per la Geodinamica Alpina e Quaternaria" is thanked for the installation and operation of the electron microprobe laboratory and "MURST ex 40%" for financial support.

#### References

- BECCALUVA, L., BIGIOGGERO, B., CHIESA, S., COLOMBO, A., FANTI, G., GATTO, G.O., GREGNANIN, A., MONT-RASIO, A. and TUNESI, A. (1983): Post-collisional orogenic dyke magmatism in the Alps. *Mem. Soc. Geol. It.* 26, 341–359.
- BELL, T.H. (1981): Foliation development: the contribution, geometry and significance of progressive bulk inhomogeneous shortening. *Tectonophysics* 75, 273–296.
- BELL, T.H. and HAYWARD, N. (1991): Episodic metamorphic reactions during orogenesis: the control of deformation partitioning on reaction sites and reaction duration. *J. Metamorphic Geol.* 9, 619–640.
- BELL, T.H. and RUBENACH, M.J. (1983): Sequential porphyroblast growth and crenulation cleavage development during progressive deformation. *Tectonophysics* 92, 171–194.
- BELL, T.H., RUBENACH, M.J. and FLEMING, P.D. (1986): Porphyroblast nucleation, growth and dissolution in regional metamorphic rocks as a function of deformation partitioning during foliation development. *J. Metamorphic Geol.* 4, 37–67.
- BIERMANN, C. (1977): The formation of sheaf-like aggregates of hornblende in Garbenschiefer from the central Scandinavian Caledonides. *Tectonophysics* 39, 487–499.
- BOHLEN, S.R. and BOETTCHER, A.L. (1982): The quartz-coesite transformation: a pressure determination and the effects of other components. *J. Geophys. Res.* 87, 7073–7078.
- BUSSY, F., VENTURINI, G., HUNZIKER, J. and MARTINOTTI, G. (1998): U–Pb ages of magmatic rocks of the western Austroalpine Dent-Blanche-Sesia Unit. *Schweiz. Mineral. Petrogr. Mitt.* 78, 163–168.
- CASTELLI, D. (1991): Eclogitic metamorphism in carbonate rocks: the example of impure marbles from the Sesia-Lanzo Zone, Italian Western Alps. *J. Metamorphic Geol.* 9, 61–77.
- COLEMAN, R.G., BEATTY, L.B. and BRANNOCK, W.W. (1965): Eclogites and eclogites: their differences and similarities. *Geol. Soc. Am. Bull.* 76, 485–508.
- COLOPIETRO, M.R. and FRIEBERG, L.M. (1987): Tourmaline-biotite as a potential geothermometer for metapelites; Black Hills, South Dakota. *Abstracts with Program. Geol. Soc. Am.* 19 (7), p. 624.
- COMPAGNONI, R. (1977): The Sesia-Lanzo zone: high-pressure low-temperature metamorphism in the Austroalpine continental margin. *Rend. Soc. Ital. Mineral. Petrol.* 33, 335–374.
- COMPAGNONI, R. and MAFFEO, B. (1973): Jadeite-bearing metagranites l.s. and related rocks in the Mount Mucrone Area (Sesia-Lanzo zone, Western Italian Alps). *Schweiz. Mineral. Petrogr. Mitt.* 53, 355–378.
- COMPAGNONI, R., DAL PIAZ, G.V., HUNZIKER, J.C., GOSSO, G., LOMBARDO, B. and WILLIAMS, P.F. (1977): The Sesia-Lanzo Zone, a slice of continental crust with alpine high pressure-low temperature assemblages in the western Italian Alps. *Rend. Soc. Ital. Min. Petrol.* 33, 281–334.



- CONNOLLY, J.A.D. (1990): Multivariable phase diagrams; an algorithm based on generalized thermodynamics. *Am. J. Sci.* 290, 666–718.
- DAL PIAZ, G.V., HUNZIKER, J.C. and MARTINOTTI, G. (1972): La Zona Sesia-Lanzo e l'evoluzione tettonico-metamorfica delle Alpi Nordoccidentali interne. *Mem. Soc. Geol. Ital.* 11, 433–460.
- DAL PIAZ, G.V., VENTURELLI, G. and SCOLARI, A. (1979): Calc-alkaline to ultrapotassic post-collisional volcanic activity in the internal northwestern Alps. *Mem. Sci. Geol. Padova* 32, 4–15.
- DE CAPITANI, L., POTENZA FIORENTINI, M., MARCHI, A. and SELLA, M. (1979): Chemical and tectonic contributions to the age and petrology of the Canavese and Sesia-Lanzo "porphyrites". *Atti Soc. Ital. Sci. Nat.* 120/1–2, 151–179.
- DUCHENE, S., Blichert, T.J., LUAI, B., TELOUK, P., LARDEAUX, J.M. and ALBAREDE, F. (1997): The Lu-Hf dating of garnets and the ages of the Alpine high-pressure metamorphism. *Nature* 387/6633, 586–589.
- ELLIS, D.J. and GREEN, D.H. (1979): An experimental study on the effect of Ca upon garnet-clinopyroxene Fe-Mg exchange equilibria. *Contrib. Mineral. Petrol.* 71, 13–22.
- FRANZ, G. and SELVERSTONE, J. (1992): An empirical phase diagram for the clinozoisite-zoisite transformation in the system  $\text{Ca}_2\text{Al}_3\text{Si}_3\text{O}_{12}(\text{OH})$ – $\text{Ca}_2\text{Al}_2\text{Fe}^{3+}\text{Si}_3\text{O}_{12}(\text{OH})$ . *Am. Mineral.* 77, 631–642.
- FRANZ, G. and SMELIK, E.A. (1995): Zoisite-clinozoisite bearing pegmatites and their importance for decompressional melting in eclogites. *Eur. J. Mineral.* 7, 1421–1436.
- GAZZOLA, D., GOSSO, G., PULCRANO, E. and SPALLA, M.I. (2000): Eo-Alpine HP metamorphism in the Permian intrusives from the steep belt of the Central Alps (Languard-Campo nappe and Tonale Series). *Geodin. Acta* 13, 149–167.
- GOSSO, G. (1977): Metamorphic evolution and fold history in the eclogite micaschists of the upper Gressoney valley (Sesia-Lanzo zone, Western Alps). *Rend. Soc. Ital. Mineral. Petrol.* 33, 389–407.
- GOSSO, G., DAL PIAZ, G.V., PIOVANO, V. and POLINO, R. (1979): High pressure emplacement of early-alpine nappes, post-nappe deformations and structural levels (Internal Northwestern Alps). *Mem. Ist. Min. Geol. Padova* 32, 5–15.
- HAMMARSTROM, J. and ZEN, E.-A. (1986): Aluminum in hornblende; an empirical igneous geobarometer. *Am. Mineral.* 71, 1297–1313.
- HOBBS, B.E., MEANS, W.D. and WILLIAMS, P.F. (1976): An outline of structural geology. Wiley, 571pp.
- HOLLAND, T.J.B. (1980): The reaction albite = jadeite + quartz determined experimentally in the range 600°–1200°C. *Am. Mineral.* 65, 129–134.
- HOLLAND, T.J.B. and POWELL, R. (1990): An enlarged and updated internally consistent thermodynamic dataset with uncertainties and correlations: the system  $\text{K}_2\text{O}$ – $\text{Na}_2\text{O}$ – $\text{CaO}$ – $\text{MgO}$ – $\text{MnO}$ – $\text{FeO}$ – $\text{Fe}_2\text{O}_3$ – $\text{Al}_2\text{O}_3$ – $\text{TiO}_2$ – $\text{SiO}_2$ – $\text{C}$ – $\text{H}_2$ – $\text{O}_2$ . *J. Metamorphic Geol.* 8, 89–124.
- HOLLAND, T. and POWELL, R. (2000): AX 1.0, Software. <http://www.esc.cam.ac.uk/astaff/holland/ax.html>.
- HOLLISTER, L.S., GRISSOM, G.C., PETERS, E.K., STOWELL, H.H. and SISSON, V.B. (1987): Confirmation of the empirical correlation of Al in hornblende with pressure of solidification of calc-alkaline plutons. *Am. Mineral.* 72, 231–239.
- HY, C. (1984): Métamorphisme polyphasé et évolution tectonique dans la croûte continentale éclogeitisée: les séries granitiques et pélitiques du Monte Mucrone (zone Sesia-Lanzo, Alpes italiennes). Université Paris VI. Unpublished PhD thesis, 200 pp.
- HYNES, A. and FOREST, R.C. (1988): Empirical garnet-muscovite geothermometry in low-grade metapelites, Selwyn Range (Canadian Rockies). *J. Metamorphic Geol.* 6, 297–309.
- ILDEFONSE, B., LARDEAUX, J.M. and CARON, J.M. (1990): The behavior of shape preferred orientations in the metamorphic rocks: amphiboles and jadeites from the Monte Mucrone Area (Sesia-Lanzo Zone, Italian Western Alps). *J. Struct. Geol.* 12, 1005–1011.
- INGER, S. and RAMSBOTHAM, W. (1997): Syn-convergent exhumation implied by progressive deformation and metamorphism in the Valle dell'Orco transect, NW Italian Alps. *J. Geol. Soc. London* 154, 667–677.
- INGER, S., RAMSBOTHAM, W., CLIFF, R.A. and REX, D.C. (1996): Metamorphic evolution of the Sesia-Lanzo Zone, Western Alps: time constraints from multi-system geochronology. *Contrib. Mineral. Petrol.* 126, 152–168.
- JOHNSON, C. and RUTHERFORD, M.J. (1989): Experimental calibration of the aluminum-in hornblende geobarometer with application to Long Valley caldera (California) volcanic rocks. *Geology* 17, 837–841.
- JOHNSON, S.E. (1990): Lack of porphyroblast rotation in the Otago schists, New Zealand; implications for crenulation cleavage development, folding and deformation partitioning. *J. Struct. Geol.* 8, 13–30.
- JOHNSON, S.E. and DUNCAN, A.C. (1992): Fault identification in complexly deformed schist terrains; examples from the USA and Australia. *Tectonophysics* 216, 291–308.
- JOHNSON, S.E. and VERNON, R.H. (1995): Inferring the timing of porphyroblast growth in the absence of continuity between inclusion trails and matrix foliations; can it be reliably done? *J. Struct. Geol.* 17, 1203–1206.
- KOONS, P.O., RUBIE, D.C. and FRUEH-GREEN, G. (1987): The effects of disequilibrium and deformation on the mineralogical evolution of quartz-diorite during metamorphism in the eclogite facies. *J. Petrol.* 28, 679–700.
- KRETZ, R. (1973): Kinetics of crystallization of garnet at two localities near Yellowknife. *Can. Mineral.* 12, 1–20.
- KRETZ, R. (1983): Symbols for rock-forming minerals. *Am. Mineral.* 68, 277–279.
- KRETZ, R. (1994): *Metamorphic Crystallization*. Wiley, 507 pp.
- KROGH, E.J. (1988): The garnet-clinopyroxene Fe-Mg geothermometer; a reinterpretation of existing experimental data. *Contrib. Mineral. Petrol.* 99, 44–48.
- LARDEAUX, J.M. and SPALLA, M.I. (1991): From granulites to eclogites in the Sesia zone (Italian Western Alps): a record of the opening and closure of the Piedmont ocean. *J. Metamorphic Geol.* 9, 35–59.
- LIU, J.G., ZHANG, R., ERNST, W.G., LIU, J. and MCLIMANS, R. (1998): Mineral parageneses in the Piampaludo eclogitic body, Gruppo di Voltri, Western Ligurian Alps. *Schweiz. Mineral. Petrogr. Mitt.* 78, 317–335.
- LIU, J., BOHLEN, S.R. and ERNST, W.G. (1996): Stability of hydrous phases in subducting oceanic crust. *Earth Planet. Sci. Lett.* 143, 161–171.
- MARUYAMA, S., CHO, M. and LIU, J.G. (1986): Experimental investigations of blueschist-greenschist transition equilibria: Pressure dependence of  $\text{Al}_2\text{O}_3$  contents in sodic amphiboles – A new geobarometer. *Geol. Soc. Am. Mem.* 164, 1–16.
- MASSONNE, H.J. and SCHREYER, W. (1987): Phengite geobarometry based on the limiting assemblage

- with k-feldspar, phlogopite and quartz. *Contrib. Mineral. Petrol.* 96, 212–224.
- MORIMOTO, N. (1988): Nomenclature of pyroxenes. *Mineral. Mag.* 52, 535–550.
- OTTEN, M.T. (1984): The origin of brown hornblende in the Artfjællet gabbro and dolerites. *Contrib. Mineral. Petrol.* 86, 189–199.
- PARK, R.G. (1969): Structural correlations in metamorphic belts. *Tectonophysics* 7, 323–338.
- PASSCHIER, C.W., MYERS, J.S. and KRÖNER, A. (1990): Field geology of high-grade gneiss terrains. Springer Verlag, 150 pp.
- PASSCHIER, C.W. and TROUW, R.A.J. (1996): *Microtectonics*. Springer Verlag, 289 pp.
- PASSCHIER, C.W., URAI, J.L., VAN LOON, J. and WILLIAMS, P.F. (1981): Structural geology of the Central Sesia-Lanzo Zone. *Geol. Mijnbouw* 60, 497–507.
- PERCHUK, L.L. (1991): Progress in metamorphic and magmatic petrology; a memorial volume in honor of D. S. Korzhinskiy. Univ. Press. Cambridge, United Kingdom.
- POGNANTE, U. (1991): Petrological constraints on the eclogite- and blueschist-facies metamorphism and P-T-t paths in the Western Alps. *J. Metamorphic Geol.* 9, 5–17.
- POGNANTE, U., COMPAGNONI, R. and GOSSO, G. (1980): Micro-mesostructural relationships in the continental eclogitic rocks of the Sesia-Lanzo zone: a record of a subduction cycle (Italian Western Alps). *Rend. Soc. Ital. Mineral. Petrol.* 36, 169–186.
- POLI, S. (1993): The amphibolite-eclogite transformation: an experimental study on basalt. *Am. J. Sci.* 293, 1061–1107.
- POWELL, R. and HOLLAND, T.J. (1985): An internally consistent thermodynamic dataset with uncertainties and correlations: 1. Methods and worked examples. *J. Metamorphic Geol.* 3, 327–342.
- RAMSAY, J.G. (1967): *Folding and Fracturing of Rocks*. McGraw-Hill, 568 pp.
- RESBAND, W. (2001): NiH Image 1.62. National Institutes of Health, USA <http://rsb.info.nih.gov/nih-image/index.html>.
- RIDLEY, J. (1989): Structural and metamorphic history of a segment of the Sesia-Lanzo Zone, and its bearing on the kinematics of Alpine deformation in the Western Alps. Conference on Alpine tectonics. *Geol. Soc. London Spec. Publ.* 45, 189–201.
- RUBATTO, D. (1998): Dating of pre-Alpine magmatism, Jurassic ophiolites and Alpine subductions in the Western Alps. Unpublished Ph.D. thesis, Swiss Federal Institute of Technology, Zürich, 174 pp.
- RUBATTO, D., GEBAUER, D. and COMPAGNONI, R. (1999): Dating of eclogite-facies zircons; the age of Alpine metamorphism in the Sesia-Lanzo Zone (Western Alps). *Earth Planet. Sci. Lett.* 167, 141–158.
- RUFFET, G., GRUAU, G., BALLEVRE, M., FERAUD, G. and PHILIPPOT, P. (1997): Rb–Sr and  $^{40}\text{Ar}$ – $^{39}\text{Ar}$  laser probe dating of high-pressure phengites from the Sesia Zone (Western Alps); underscoring of excess argon and new age constraints on the high-pressure metamorphism. *Chem. Geol.* 141, 1–18.
- SCHMIDT, M.W. (1993): Phase relations and compositions in tonalite as a function of pressure: an experimental study at 650°C. *Am. J. Sci.* 293, 1011–1060.
- SPALLA, M.I., DE MARIA, L., GOSSO, G., MILETTO, M. and POGNANTE, U. (1983): Deformazione e metamorfismo della Zona Sesia-Lanzo meridionale al contatto con la falda piemontese e con il massiccio di Lanzo, Alpi occidentali. *Mem. Soc. Geol. Ital.* 26, 499–514.
- SPALLA, M.I., LARDEAUX, J.M., DAL PIAZ, G.V. and GOSSO, G. (1991): Metamorphisme et tectonique a la marge externe de la zone Sesia-Lanzo (Alpes occidentales). *Mem. Soc. Geol. Ital.* 43, 361–369.
- SPALLA, M.I. and GOSSO, G. (1999): Pre-Alpine tectono-metamorphic units in the central Southern Alps: structural and metamorphic memory. In: 3rd Workshop on Alpine Geological Studies. *Mem. Sci. Geol.* 51, 221–229.
- SPALLA, M.I., LARDEAUX, J.M., DAL PIAZ, G.V., GOSSO, G. and MESSIGA, B. (1996): Tectonic significance of Alpine eclogites. *J. Geodin.* 21, 257–285.
- SPALLA, M.I., SILETTO, G.B., DI PAOLA, S. and GOSSO, G. (2000): The role of structural and metamorphic memory in the distinction of tectono-metamorphic units: the basement of the Como lake in the Southern Alps. *J. Geodin.* 30, 191–204.
- SPEAR, F. (1993): Metamorphic phase equilibria and pressure-temperature-time paths. *Min. Soc. Am.*, 799 pp.
- STÜNITZ, H. (1989): Partitioning of metamorphism and deformation in the boundary region of the “Seconda Zona Diorito-Kinzigitica”, Sesia Zone, Western Alps. Unpublished Ph.D. thesis ETH, Zürich, 248 pp.
- THOMPSON, A.B. (1976): Mineral reactions in pelitic rocks I. Predictions of P-T-X (Fe-Mg) phase relations. II. Calculation of some P-T-X (Fe-Mg) phase relations. *Am. J. Sci.* 276, 201–254.
- TURNER, F.J. and WEISS, L.E. (1963): *Structural analysis of metamorphic tectonites*. MacGraw-Hill, 545 pp.
- TWISS, R.J. and MOORE, C.H. (1993): *Structural Geology*. Freeman, 532 pp.
- VAN ROERMUND, H., LISTER, G. and WILLIAMS, P.F. (1979): Progressive development of quartz fabrics in a shear zone from Monte Muçrone, Sesia-Lanzo Zone, Italian Alps. *J. Struct. Geol.* 1, 43–52.
- VENTURINI, G. (1995): Geology, geochemistry and geochronology of the inner central Sesia Zone (Western Alps, Italy). *Mém. de Geol. Lausanne* 25, 148 pp.
- VENTURINI, G., MARTINOTTI, G., ARMANDO, G., BARBERO, M. and HUNZIKER, J.C. (1994): The Central Sesia Lanzo Zone (western Italian Alps); new field observations and lithostratigraphic subdivisions. *Schweiz. Mineral. Petrogr. Mitt.* 74, 115–125.
- VENTURINI, G., MARTINOTTI, G. and HUNZIKER, J.C. (1991): The protoliths of the “Eclogitic Micaschists” in the lower Aosta Valley (Sesia-Lanzo zone, Western Alps). *Mem. Sc. Geol.* 43, 347–359.
- VIUCHARD, J. P. (1986): Cinématique éo-alpine et alpine en zone Sesia-Lanzo (Alpes occidentales internes). *C.R.A.S. Paris II* (303), 1333–1338.
- WILLIAMS, P.F. (1985): Multiply deformed terrains – problems of correlation. *J. Struct. Geol.* 7, 269–280.
- WILLIAMS, P.F. and COMPAGNONI, R. (1983): Deformation and metamorphism in the Bard area of the Sesia-Lanzo zone, Western Alps, during subduction and uplift. *J. Metamorphic Geol.* 1, 117–140.
- ZUCALI, M. (2002): Tectonic imprints of a subduction cycle in continental rocks explicated by a foliation map of the “Eclogitic Micaschists Complex” between Monte Muçrone-Monte Mars-Mombarone (Sesia-Lanzo Zone, Austroalpine Domaine, Western Alps, Italy). *Mem. Soc. Geol. It.* 54, in press.

## Appendix

Table A1

Mineral: Rocks:	Garnet				Epidote				Kyanite		
	<i>M.pelites</i>	<i>M.qtzdiorites</i>	<i>M.basites</i>	<i>Quartzites</i>	<i>Metapelites</i>	<i>Metaquartzdiorite</i>			<i>Quartzites</i>		
	GrII	GrI	GrI	GrI	CzoI	CzoI	CzoII	CzoII			
SiO <sub>2</sub>	38.54	38.97	38.41	37.10	SiO <sub>2</sub>	39.74	39.19	38.64	39.11	SiO <sub>2</sub>	36.56
TiO <sub>2</sub>	0.00	0.01	0.24	0.07	TiO <sub>2</sub>	0.04	0.22	0.18	0.23	TiO <sub>2</sub>	0.03
Al <sub>2</sub> O <sub>3</sub>	21.60	21.75	20.93	20.83	Al <sub>2</sub> O <sub>3</sub>	32.05	29.04	28.08	27.61	Al <sub>2</sub> O <sub>3</sub>	62.37
FeO	23.42	23.77	25.96	33.87	Fe <sub>2</sub> O <sub>3</sub> *	1.94	6.61	7.48	8.68	Fe <sub>2</sub> O <sub>3</sub> *	1.13
MnO	0.40	0.36	0.71	0.91	MnO	0.00	0.01	0.04	0.2	MnO	0.02
MgO	4.93	7.73	4.64	2.56	MgO	0.04	0.1	0.03	0.08	MgO	0.01
CaO	11.24	7.50	9.24	4.87	CaO	24.76	23.1	22.91	22.62	CaO	0.02
Na <sub>2</sub> O	0.00	0.01	0.00	0.00	Na <sub>2</sub> O	0.03	0.01	0.00	0.01	Na <sub>2</sub> O	0.00
K <sub>2</sub> O	0.00	0.01	0.00	0.00	K <sub>2</sub> O	0.02	0.01	0.00	0.03	K <sub>2</sub> O	0.01
Totals	100.14	100.11	100.13	100.21	Totals	98.62	98.29	97.38	98.57	Totals	100.15
Si	2.99	2.99	3.00	2.98	Si	3.01	3.01	3.01	3.02	Si	1.98
Ti	0.00	0.00	0.01	0.00	Ti	0.00	0.01	0.01	0.01	Ti	0.00
Al	1.97	1.97	1.93	1.97	Al	2.86	2.63	2.58	2.52	Al	3.98
Fe <sup>3+</sup>	0.05	0.06	0.04	0.07	Fe <sup>3+</sup>	0.11	0.38	0.44	0.51	Fe <sup>3+</sup>	0.05
Fe <sup>2+</sup>	1.46	1.46	1.66	2.19	Mn	0.00	0.00	0.00	0.01	Mn	0.00
Mn	0.03	0.02	0.05	0.06	Mg	0.01	0.01	0.00	0.01	Mg	0.00
Mg	0.57	0.88	0.54	0.31	Ca	2.01	1.95	1.92	1.87	Ca	0.00
Ca	0.93	0.62	0.78	0.42	Na	0.00	0.00	0.00	0.00	Na	0.00
Na	0.00	0.00	0.00	0.00	K	0.00	0.00	0.00	0.00	K	0.00
K	0.00	0.00	0.00	0.00	<b>Al2Fe</b>	<b>11</b>	38	43	50		
<b>Alm</b>	0.49	0.49	0.55	0.74							
<b>Prp</b>	0.19	0.30	0.18	0.10							
<b>Grs</b>	0.31	0.21	0.26	0.14							

Table A2

Mineral: Rocks:	Chloritoid			Clinopyroxene				
	<i>Quartzites</i>			<i>Metaquartzdiorites</i>		<i>Metapelites</i>		
	cldI core	cldI rim	cldII	OmpI rim	OmpI core	OmpI	OmpII	
SiO <sub>2</sub>	24.39	24.65	25.01	SiO <sub>2</sub>	55.99	52.97	55.81	55.89
TiO <sub>2</sub>	0.00	0.02	0.00	TiO <sub>2</sub>	0.03	0.01	0.09	0.07
Al <sub>2</sub> O <sub>3</sub>	42.04	42.27	41.33	Al <sub>2</sub> O <sub>3</sub>	10.89	10.39	11.08	11.63
FeO	21.98	25.61	26.51	FeO	3.26	8.34	3.46	3.12
MnO	0.28	0.34	0.20	MnO	0.03	0.05	0.02	0.04
MgO	4.89	2.74	2.76	MgO	9.01	15.39	9.06	8.94
CaO	0.01	0.02	0.02	CaO	13.60	6.92	13.68	13.26
Na <sub>2</sub> O	0.00	0.00	0.00	Na <sub>2</sub> O	6.76	4.35	6.96	7.12
K <sub>2</sub> O	0.00	0.01	0.01	K <sub>2</sub> O	0.01	0.16	0.01	0.00
Totals	93.59	95.66	95.84	Totals	99.58	98.58	100.17	100.08
Si	2.28	2.29	2.33	Si	1.99	1.91	1.97	1.97
Ti	0.00	0.00	0.00	Ti	0.00	0.00	0.00	0.00
Al	4.63	4.63	4.54	Al	0.46	0.44	0.46	0.48
Fe <sup>3+</sup>	0.13	0.10	0.13	Fe <sup>3+</sup>	0.03	0.05	0.07	0.06
Fe <sup>2+</sup>	1.58	1.88	1.93	Fe <sup>2+</sup>	0.06	0.19	0.03	0.03
Mn	0.02	0.03	0.02	Mn	0.00	0.00	0.00	0.00
Mg	0.68	0.38	0.38	Mg	0.48	0.83	0.48	0.47
Ca	0.00	0.00	0.00	Ca	0.52	0.27	0.52	0.50
Na	0.00	0.00	0.00	Na	0.47	0.30	0.48	0.49
K	0.00	0.00	0.00	K	0.00	0.01	0.00	0.00
<b>X<sub>Mg</sub></b>	0.30	0.17	0.17	<b>Jd</b>	0.44	0.30	0.43	0.45
				<b>Acm</b>	0.03	0.05	0.08	0.07
				<b>Di</b>	0.46	0.27	0.47	0.46



Representative analyses of amphibole, white mica, chloritoid, clinopyroxene, garnet, epidote and kyanite from metapelites, metabasites, meta-quartzdiorites and kgrt-cld bearing quartzites. Stoichiometric ratios of elements based on 23 equivalent O for amphibole, with

$Fe^{tot}$  as  $Fe^{2+}$ , 12 for garnet, 12.5 for epidote, 10 for kyanite, 22 for white mica, 6 for pyroxene and 14 for chloritoid;  $X_{Mg} = Mg/(Mg+Fe)$ ,  $Al_2Fe = Fe/(Fe+Al-2)$ ,  $Pg = Na/(Na+K)$ .

Table A3

Mineral: Sample:	White Mica							
	Metapelites			Metaquartzdiorites		Quartzites		
	WmII/III	WmII/III	WmII/III	WmII	WmII	WmI	WmI	WmII
SiO <sub>2</sub>	52.03	36.01	53.45	49.93	52.15	51.25	50.93	48.96
TiO <sub>2</sub>	0.32	0.03	0.36	0.09	0.35	0.32	0.31	0.00
Al <sub>2</sub> O <sub>3</sub>	28.91	61.44	29.20	40.44	28.49	28.48	30.79	36.13
FeO	1.65	1.11	1.75	0.40	1.58	1.63	1.66	2.05
MnO	0.02	0.02	0.00	0.00	0.00	0.02	0.03	0.04
MgO	3.56	0.01	3.76	0.19	3.67	3.51	2.55	0.74
CaO	0.00	0.02	0.00	0.17	0.00	0.00	0.00	0.00
Na <sub>2</sub> O	1.00	0.00	0.60	5.02	0.59	0.99	0.89	0.71
K <sub>2</sub> O	10.00	0.01	7.74	0.74	7.55	9.85	9.06	8.58
Totals	97.50	97.12	96.86	96.98	94.38	96.91	96.23	97.22
Si	6.74	6.06	6.84	6.18	6.85	5.99	6.64	6.29
Ti	0.03	0.01	0.03	0.01	0.03	0.01	0.03	0.00
Al	4.42	5.87	4.40	5.90	4.41	6.04	4.74	5.47
Fe <sup>2+</sup>	0.18	0.04	0.17	0.04	0.17	0.05	0.18	0.20
Mn	0.00	0.00	0.00	0.00	0.00	0.01	0.00	0.00
Mg	0.69	0.05	0.72	0.04	0.72	0.01	0.50	0.14
Ca	0.00	0.05	0.00	0.02	0.00	0.04	0.00	0.00
Na	0.25	1.74	0.15	1.20	0.15	1.46	0.23	0.18
K	1.66	0.12	1.26	0.12	1.27	0.18	1.51	1.41
<b>Pg</b>	0.13	0.94	0.10	0.91	0.11	0.89	0.13	0.11

Table A4

Mineral: Rocks:	Amphibole								
	Metapelites				Metaquartzdiorites		Metabasites		
	AmpI/II	AmpI/II	AmpIII	AmpIV	AmpI	AmpIII	pre-Alpine	AmpII	AmpIII
SiO <sub>2</sub>	49.32	56.47	56.35	52.01	52.18	54.57	49.04	48.79	53.53
TiO <sub>2</sub>	0.17	0.04	0.04	0.07	0.13	0.03	1.66	0.30	0.02
Al <sub>2</sub> O <sub>3</sub>	10.04	11.49	11.46	7.20	10.06	4.81	8.20	9.73	4.27
FeO	12.53	12.31	12.43	14.21	9.75	9.51	10.79	13.66	13.12
MnO	0.00	0.00	0.00	0.08	0.03	0.05	0.01	0.12	0.27
MgO	14.08	9.48	9.45	12.97	14.52	17.19	15.83	13.74	15.11
CaO	7.86	1.63	1.62	8.98	6.82	10.24	9.06	9.20	10.39
Na <sub>2</sub> O	4.15	6.86	6.85	2.69	4.10	1.91	3.00	3.01	1.68
K <sub>2</sub> O	0.24	0.04	0.04	0.17	0.25	0.15	0.57	0.52	0.08
Totals	98.39	98.32	98.25	98.38	97.84	98.46	98.16	99.07	98.47
Si	7.01	7.80	7.79	7.42	7.29	7.61	6.97	6.95	7.60
Ti	0.02	0.00	0.00	0.01	0.01	0.00	0.18	0.03	0.00
Al	1.68	1.87	1.87	1.21	1.66	0.79	1.37	1.63	0.72
Fe <sup>2+</sup>	1.44	1.41	1.42	1.67	1.10	1.08	1.24	1.58	1.53
Mn	0.00	0.00	0.00	0.01	0.00	0.01	0.00	0.01	0.03
Mg	2.98	1.95	1.95	2.76	3.05	3.57	3.35	2.92	3.20
Ca	1.20	0.24	0.24	1.37	1.02	1.53	1.38	1.40	1.58
Na	1.14	1.84	1.84	0.74	1.11	0.52	0.83	0.83	0.46
K	0.04	0.01	0.01	0.03	0.05	0.03	0.10	0.10	0.02
<b>X<sub>Mg</sub></b>	0.67	0.58	0.58	0.62	0.73	0.77	0.73	0.65	0.68